CFD Letters

Optimising Biogas Utilisation from Palm Oil Mill Effluent in Dual-Fuel Engines: A CFD Simulation Approach

Chen Yie Yong[1,*], Andrew Ragai Henry Rigit[1], Khairuddin Sanaullah[2]

[1] Department of Mechanical and Manufacturing Engineering, Faculty of Engineering, Universiti Malaysia Sarawak, 94300, Kota Samarahan, Sarawak, Malaysia
[2] Discipline of Chemical Engineering, School of Engineering, University of KwaZulu-Natal, Durban, South Africa

ARTICLE INFO	ABSTRACT
	The transition towards sustainable energy is crucial for mitigating climate change and reducing dependence on limited fossil fuels. This study aims to optimise the utilisation of biogas generated from palm oil mill effluent (POME) in dual fuel engines through computational fluid dynamics (CFD) simulation. However, this study addressed the challenge of variation in the composition of raw biogas. These differences may make it difficult to effectively control the combustion of internal combustion engines. Thus, to overcome this challenge, the composition of biogas is fixed throughout the cleaning and reforming stages in this study. Using a three-dimensional computational model to evaluate the operation of a single-cylinder compression ignition engine at 1300 rpm under traditional diesel and dual fuel conditions. Due to the symmetry of the cylinder and the periodic pattern of the injector nozzle holes, a 60-degree sector grid representing one-sixth of the cylinder was selected to simulate the entire geometric shape. Using ANSYS Forte software for CFD combustion simulation, this study investigates the effects of reforming biogas substitution on the indicated average effective pressure, total power, thermal efficiency, combustion efficiency and emission characteristics of nine different biogas diesel components (from 0% to 0%). 80% biogas substitution is 20% step size. The research results indicate that replacing diesel with gas fuels such as reformed biogas in dual-fuel engines can affect the performance and efficiency of the engine. Although combustion efficiency and thermal efficiency may initially increase, they will significantly decrease at higher substitution rates, especially at 80%. Nevertheless, reforming biogas still has advantages such as reducing emissions and maintaining output power at medium to high loads. However, compared to traditional diesel engines, challenges such as decreased volumetric efficiency and indicated mean effective pressure (IMEP) lead to an overall decline in engine performance.

1. Introduction

The transition to renewable energy is crucial for combating climate change, yet Malaysia's heavy reliance on fossil fuels, comprising 94% of energy consumption in 2019, remains a challenge. The palm oil industry, a cornerstone of Malaysia's economy, offers a potential solution through the large-

scale production of palm oil mill effluent (POME), which can be converted into biogas. However, integrating POME-derived biogas into diesel engines faces hurdles due to fluctuating composition and limited fluid dynamics understanding. Hence, the research focuses on using Computational Fluid Dynamics (CFD) simulations to optimise combustion in dual-fuel engines to overcome this issue [8]. By developing a tailored CFD model, assessing different biogas compositions' impact and fine-tuning combustion variables, such as temperature and air-fuel ratio, the study aims to enhance engine performance while minimising emission characteristics. This iterative approach seeks to identify optimal combustion parameters, advancing renewable energy technology and sustainability within the palm oil sector.

The literature review highlights the potential of POME-derived biogas in gas engines and explores various methods to optimize combustion processes, primarily through modelling and experimental approaches. Mahmoodi *et al.,* [21] emphasised the challenges in controlling combustion variations, while Gupta *et al.,* [13] focused on optimising biogas compositions for improved performance. Ravi Chandran *et al.,* [23] demonstrated the effectiveness of CFD simulations, especially in evaluating an 80/20 biogas-diesel blend's combustion efficiency. Similarly, Bundele *et al.,* [7] explored blending hydrogen with biogas, noting benefits but also increased emissions. Alrbai *et al.,* [2] addressed the role of trace elements in engine performance, advocating further research to maximize environmental advantages. Hussain *et al.,* [19] showed that using biogas as a dual fuel with diesel reduces emissions and improves efficiency, supported by CFD analysis and experimental validation. Additionally, Feroskhan *et al.,* [9] reported that biogas can replace up to 90% of diesel input, cutting diesel consumption by 67%, with significant emission reductions—75% less smoke and 55% less NOx. Methane enrichment and intake heating further improve brake thermal efficiency (BTE) and reduce fuel use. Despite biogas' lower reactivity, its use in dual-fuel systems shows promise for reducing diesel reliance. Ismail *et al.,* [16] complements these findings by investigating the effects of recirculation ratios on biogas combustion in a flameless combustor, showing that higher ratios improve flame stability and reduce NOx and CO emissions. Finally, Ghenai *et al.,* [10] provided a broader perspective on biofuels, stressing their environmental benefits and the need for better infrastructure to support their adoption. Together, these studies underline the effectiveness of biogas in reducing emissions and improving engine performance, positioning it as a promising alternative fuel source. For the methodology, a three-dimensional computational model was utilised to test a compression ignition engine's dual-fuel operations at 1300 rpm. Due to the symmetry of the cylinder and the periodic pattern of the injector nozzle holes, a 60-degree sector grid representing one-sixth of the cylinder was selected to simulate the complete geometry. CFD combustion simulation was performed using ANSYS Forte software to examine the effects of reformed biogas substitution on indicated mean effective pressure, gross indicated power, thermal efficiency, combustion efficiency and emission characteristics. This study was performed for five different biogas-diesel compositions, ranging from 0% to 80% biogas substitution in 20% increments.

On top of that, despite significant research that has been made regarding the utilisation of biogas in combustion engine applications, there are still several key gaps in current research that need to be addressed to utilise its potential fully. Firstly, the impact of biogas composition variability is a major area that needs further exploration. At present, previous research is mainly focused on the carbon dioxide (CO_2) and methane (CH_4) content of biogas, but there is less attention paid to the effects of trace elements such as ammonia (NH_3), hydrogen sulphide (H2S), oxygen (O_2), carbon monoxide (CO), nitrogen (N_2) and water (H_2O) [2]. The impact of these trace elements on combustion characteristics, engine performance and emissions are yet to be fully understood. It is necessary to comprehensively study the effects of these elements on different types of engines and operating conditions to optimise engine performance and emissions for various biogas compositions [15].

Another significant gap is the understanding of cycle-to-cycle variability (CCVs) in combustion. These variations are largely influenced by the composition of biogas, which in turn affects the stability and noise of the engine. Although a previous study has explored the impact of CO2 levels on CCVs, there is still a lack of detailed research to examine how the broader composition of biogas affects these variations [13]. Hence, the research is important for improving the durability, performance and noise control of engines using biogas. Apart from that, there is also a research gap in the dual fuel combustion strategy, especially in exploring the substitution ratio of biogas diesel dual fuel engines to optimise their performance and emission. Another previous study shows the efficiency of dual fuel mode under different loads, especially partial loads, has not been fully explored [23]. Hence, it is necessary to develop strategies for using various biogas components to enhance the stability and performance of dual-fuel engines. This research gap limits the optimisation of dual fuel strategies in practical applications.

Although some studies have been made in developing chemical kinetics and multi-zone models for biogas combustion, more complex models are needed to integrate detailed CFD [2,29]. These advanced models can more accurately predict the combustion process and optimise engine performance under different conditions. Understanding flame dispersion and emission characteristics through these models is crucial for advancing biogas combustion technology. Additionally, research on biogas-hydrogen mixtures has shown the potential ability to improve combustion efficiency and reduce emissions [7]. However, further research is needed to optimise the conditions for hydrogen mixing, understand its long-term impact on engine durability and evaluate its economic feasibility [4,6]. Addressing these issues is crucial for fully utilising the advantages of biogas-hydrogen mixtures. Emission control is also an area that requires more detailed analysis. Although biogas combustion can reduce nitrogen oxide (NO_x) emissions by lowering combustion temperature, further research is needed on the formation of other pollutants such as sulphur oxide (SO_x) and particulate matter, especially with changes in biogas composition [28]. In addition, evaluating the effectiveness of different post-treatment technologies in biogas fuel engines is significant for comprehensive emission control strategies [1,27,31]. Finally, the economic and environmental trade-offs of using biogas require more comprehensive documentation. Although biogas provides significant environmental benefits, the economic impact of upgrading biogas to biomethane and the associated costs of dual fuel systems have not been fully documented [7]. A comprehensive cost-benefit analysis is needed, taking into account economic and environmental impacts, to make biogas a feasible alternative to fossil fuels.

Addressing these research gaps is of great environmental, economic and technological significance for advancing our understanding and optimisation of biogas combustion in engines. From an environmental perspective, utilising biogas as a renewable energy source can significantly reduce greenhouse gas emissions compared to fossil fuels [30]. Optimising the biogas combustion process can enhance these environmental benefits and contribute to global efforts to mitigate climate change. In terms of energy security, developing efficient biogas combustion technologies can reduce dependence on fossil fuels, thereby promoting energy security and sustainability. This is particularly important for biogas production in areas with abundant biomass resources, providing a decentralised renewable energy solution [20]. In terms of economy, addressing the high costs associated with upgrading biogas and optimising combustion technology can make biogas a more feasible alternative. This includes reducing engine modification costs, improving fuel efficiency and developing cost-effective dual fuel systems. A comprehensive cost-benefit analysis will help to understand the full economic potential of biogas. By improving the understanding of biogas combustion kinetics, especially under different compositions and hydrogen-rich conditions, engine performance and durability can be significantly improved. This can lead to more stable and efficient

engines, especially in dual fuel and advanced combustion modes such as homogeneous compression ignition (HCCI). Therefore, the objectives of this research are:

i. To develop a detailed Computational Fluid Dynamics (CFD) model for simulating the combustion of biogas from Palm Oil Mill Effluent (POME) in dual-fuel engines.
ii. To assess how different biogas compositions affect the optimum combustion conditions using CFD simulations.
iii. To optimise the combustion system by adjusting variables including inlet temperature, intake pressure and air-fuel ratio and evaluating engine performance.

In short, improving combustion and thermal efficiencies by switching from diesel to gaseous fuels such as reformed biogas in dual-fuel engines might potentially result in decreased volumetric efficiency and engine performance. Reformed biogas has the potential to reduce emissions without substantially impairing engine output power, particularly at medium to high loads, according to the study, which emphasises the sensitive trade-off between these parameters. For internal combustion engines to operate as efficiently as possible, fuel blending schemes require further study.
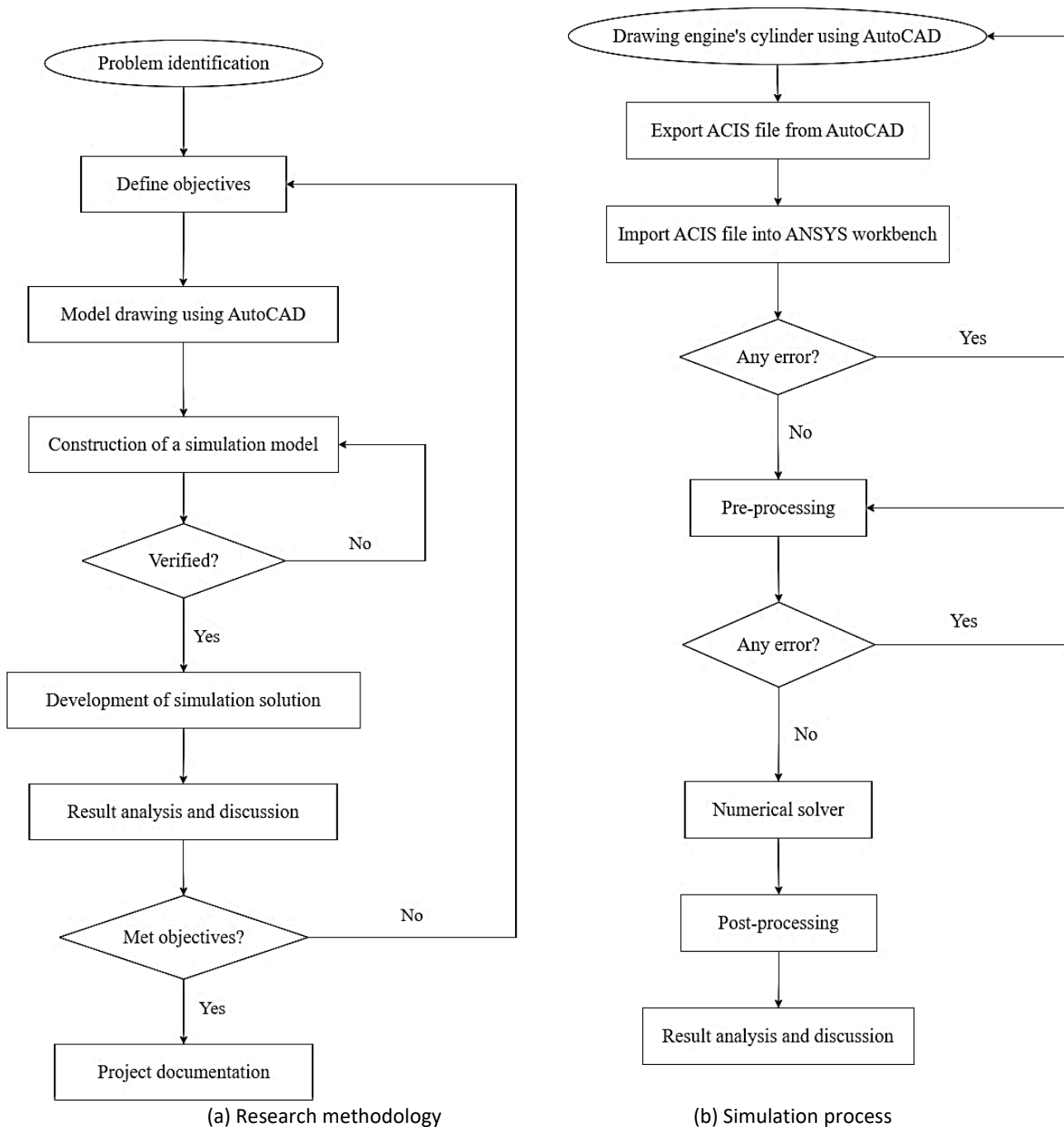
2. Methodology
2.1 Description of Methodology

The simulation process begins with defining the research problem, which focuses on evaluating the performance of dual-fuel engines using biogas and diesel. A combustion model, referenced from existing studies, is employed and a Sector Mesh Generator tool is used to create a 60-degree sector grid with a body-fitted mesh. After running the simulation, the results will be analysed to assess the feasibility of the turbine across different locations and achieve the study's objectives. The flow of research methodology is shown in Figure 1(a).

Data collection for the study draws from previous research, particularly regarding POME characteristics, combustion details and engine specifications. Utilizing pre-existing data helps save time and resources but introduces potential limitations like biases, inconsistencies between studies and limitations in data relevance for specific scenarios. MATLAB software is used for statistical analysis and optimization, though its steep learning curve and computational intensity pose challenges.

For the CFD simulations, ANSYS is employed to model the combustion process in dual-fuel engines. The numerical study includes three stages: pre-processing, solving and post-processing. ANSYS Forte is used to analyse parameters like thermal efficiency, temperature distribution and pressure profiles. However, the complexity of ANSYS requires specialized knowledge and the simulations demand significant computational resources. Additionally, assumptions and simplifications in CFD models may limit accuracy, particularly in capturing the intricacies of the combustion process. The simulation flow is illustrated in Figure 1(b).

(a) Research methodology   (b) Simulation process
Fig. 1. Flow chart of the (a) Research methodology (b) Simulation process

2.2 Engine Specifications

The reference engine used for the analysis was a common rail direct-injector direct-injection diesel engine manufactured by Caterpillar PRIME, whose main characteristics are listed in Table 1 and Table 2.

Table 1
Reference dual fuel engine specifications

Specification	Description
Engine type	Caterpillar PRIME 648ekW 810kVA (4-stroke cycle, water-cooled diesel)
Governor type	PEEC- Cat Electronic
Displacement (per cylinder)	2439cc
Bore x Stroke	165.1mm x 137.16mm
Connecting rod length	26.16mm
Speed	1300rpm
IVC (°ATDC)	-95 degrees
EVO (°ATDC)	130 degrees
Power factor	0.8
Compression Ratio	16:1

Table 2
Common rail direct-injector specifications

Specifications	Description
No. of holes	7
Hole diameter (mm)	0.141
Included spray angle (°)	148
Geometric area (mm^2)	0.1093

2.3 Fuel Properties
2.3.1 Reformed biogas and diesel

Hydrogen gas (H_2), hydrogen sulphide (H_2S), CH_4, CO_2, N_2, O_2, CO and H_2O can all be found in POME derived biogas. In the POME-derived biogas, H_2S is present in negligible amounts while CH_4 and CO_2 are present in the largest concentrations [25]. Although the other ingredients are little, they have an impact on how biogas and diesel burn. It is therefore impossible to forecast with any degree of accuracy how biogas will burn in an internal combustion engine. In the current study, the H_2S was initially extracted on a bed of mixed ferric oxide (Fe_2O_3) and then collected as follows [14]:

$$Fe_2O_3 + 3H_2S \rightarrow Fe_2S_3 + 3H_2O \tag{1}$$

The CO2 was eliminated using a Pressure Swing Absorption (PSA) membrane after the hydrogen sulphide was eliminated [26]. In order to prevent lowering the catalytic efficiency in the subsequent stages, the H_2:CO ratio has to be adjusted before the reforming stage using a water gas shift (WGS) reactor and a PSA membrane [22]. Ultimately, CH_4 in biogas combines with air and water in the reformer to produce CO, CO_2, H_2, N_2 and H_2O, which are then used as the final product for port fuel injection in the intake manifold of Caterpillar PRIME engines. The reactions of modifying are stated below :

$$CH_4 + H_2O \leftrightarrow CO + 3H_2 \qquad \Delta H°_{298K} = 206 \, kJ/mol \tag{2}$$

$$CH_4 + 2O_2 + N_2 \leftrightarrow CO_2 + 2H_2O + N_2 \quad \Delta H°_{298K} = -802 \, kJ/mol \tag{3}$$
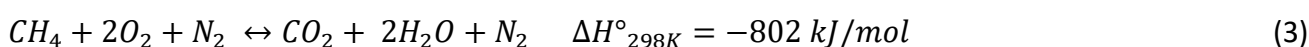
The engine simulations maintained a constant input total energy of 5100 J/cycle. The mass flow of dodecane ($C_{12}H_{26}$) and reformed biogas varied based on their lower heat values (LHV) and the

reformed biogas substitution ratio. In addition, the crucial properties of fuels that have been used in the simulations are tabulated in Table 3.

Table 3
Properties of the fuels

Properties	Diesel	Reformed Biogas
Chemical structure	$C_{12}H_{26}$	Mole fraction: 0.2060 H_2; 0.1376 CO; 0.1064 H_2O; 0.0187 CO_2;0.5312 N_2
Density (kg/m^3)	743.72 at 300K	0.1037 at 350K
Lower heating value (MJ/kg)	42500	4060.00

2.3.2 Reformed biogas substitution

In every scenario, the engine speed and the total fuel energy input were maintained at 1300 revolutions per minute and 5100 joules per cycle, respectively. The ratio of the reformed energy input rate to the total fuel energy delivered to the engine per cycle is known as the reformed biogas substitution ratio [18]. The reformed biogas substitution ratio is calculated as:

$$Biogas\ Substituation\ Ratio = \frac{\dot{m}_{biogas}LHV_{biogas}}{\dot{m}_{biogas}LHV_{biogas}+\dot{m}_{diesel}LHV_{diesel}} \times 100\% \tag{4}$$

where, $\dot{m}_{biogas}$ *and* $\dot{m}_{diesel}$ are the mass flow rates of reformed biogas and diesel fuel in g/cycle, respectively. LHV_{biogas} and LHV_{diesel} refer to the lower heating value of the reformed biogas and diesel fuel in MJ/kg entering the engine, respectively [15,21]. The calculation of the reformed biogas substitution ratio is tabulated in Table 4.

Table 4
Calculation of reformed biogas substitution ratio

Reformed biogas		Diesel		Reformed biogas substitution ratio (%)
Lower heating value (kJ/m^3)	Mass flow rate (g/cycle)	Lower heating value (kJ/m^3)	Mass flow rate (g/cycle)	
4060.00	0	42500.00	0.1200	0
	0.2512		0.0960	20.0
	0.5024		0.0720	40.0
	0.7535		0.0480	60.0
	1.0045		0.0240	80.0

2.4 Governing Equations
2.4.1 Species conservation equation

In combustion engines, the gas-phase working fluids consist of a mixture of different gas components or species. The composition of these species' changes during the engine cycle due to various processes, including combustion, turbulent transport, convection and molecular diffusion. The mass conservation of these species is represented by the species conservation equation [3]:

$$\frac{\partial \overline{\rho}_k}{\partial t} + \nabla \cdot (\bar{\rho}_k \widetilde{\boldsymbol{u}}) = \nabla \cdot [\bar{\rho}D\nabla \bar{y}_k] + \nabla + \Phi \ (k = 1, \dots, K) \tag{5}$$

where $\bar{\rho}_k$ is the density, subscript k is the species index, K is the total number of species, $\boldsymbol{u}$ and is the flow velocity vector. The Φ term accounts for convection and source terms due to chemical reactions and spray evaporation.

2.4.2 Fluid continuity equation

The summation of the species conservation equation for all species results in the continuity equation for the total gas-phase fluid [3]:

$$\frac{\partial \bar{\rho}}{\partial t} + \nabla \cdot (\bar{\rho}\tilde{\boldsymbol{u}}) = \dot{\bar{\rho}}^S \tag{6}$$

This equation ensures the conservation of mass within the system.

2.4.3 Momentum conservation equation

The momentum conservation equation considers various forces, including convection, pressure force, viscous stress, turbulent transport and body forces. It is expressed by ANSYS Inc. [3]:

$$\frac{\partial \bar{\rho}\tilde{\boldsymbol{u}}}{\partial t} + \nabla \cdot (\bar{\rho}\tilde{\boldsymbol{u}}\tilde{\boldsymbol{u}}) = -\nabla \bar{p} + \nabla \cdot \bar{\sigma} - \frac{2}{3}\bar{\rho}\tilde{k}\boldsymbol{I} + \overline{\boldsymbol{F}^s} + \overline{pg} \tag{7}$$

where p is the pressure, F^s refers to the rate of momentum gain due to sprays, g is the specific body force and $\bar{\sigma}$ is the viscous shear stress.

2.4.4 Energy conservation equation

According to the First Law of Thermodynamics, the change in internal energy must be balanced by pressure work and heat transfer. For combustion engines, the energy conservation equation incorporates the effects of convection, turbulent transport, dissipation, sprays and chemical reactions. It is represented by ANSYS Inc. [3]:

$$\frac{\partial \bar{\rho}\bar{I}}{\partial t} + \nabla \cdot (\bar{\rho}\tilde{\boldsymbol{u}}\tilde{I}) = \bar{\rho}\nabla \cdot \tilde{\boldsymbol{u}} - \nabla \cdot \bar{\boldsymbol{J}} - \nabla \cdot \boldsymbol{H} + \bar{\rho}\tilde{\varepsilon} + \dot{\bar{Q}}^C + \dot{\bar{Q}}^S \tag{8}$$

where I is the specific internal energy, J is the heat flux vector accounting for contributions due to heat conduction and enthalpy diffusion, while $\dot{\bar{Q}}^C$ and $\dot{\bar{Q}}^S$ represent chemical and spray heat sources.

2.4.5 Gas-phase mixture equation of state

For gas-phase mixtures, the ideal gas law is assumed, with thermodynamic relations following the Dalton model. Under this assumption, each gas component behaves as an ideal gas at a specific temperature $\tilde{T}$ and volume [3]. The equation of state is given by ANSYS Inc. [3]:

$$\bar{p} = R_u \tilde{T} \sum_k \left(\frac{\bar{\rho}_k}{W_k}\right) \tag{9}$$

where R_u is the universal gas constant and W_k is the molecular weight of species k.

2.4.6 Chemical kinetics formulation

The chemical kinetics governing combustion are expressed using reversible and irreversible reactions. The species production rate and corresponding heat release contribute to the continuity and energy equations [3]:

$$\sum_{k=1}^{K} V'_{ki}\chi_k \Longleftrightarrow \sum_{k=1}^{K} V''_{ki}\chi_k \qquad (i = 1, \dots, I) \tag{10}$$

The source term for chemical reactions is added to the species conservation equation. This research used a pre-installed chemistry set included with Forte employed in the chemistry model [24]. This chemistry-set file (.cks) is a conventional CHEMKIN file with a simplified system designed for dual-fuel settings.

2.5 CFD Simulation using ANSYS Forte IC Engine Software
2.5.1 Developing geometry

Since the cylinder symmetry and the periodicity of injector nozzle hole patterns may be used, a 60-degree sector grid (1/6 of the cylinder) was selected to represent the complete geometric shape. To save computational time and achieve a feasible completion date for this project, a sector grid is used as the computational domain for the combustion chamber. The Sector Mesh Generator tool uses body-fitted grid calculation to construct a 60-degree sector grid. The visualization of sector mesh geometry in Forte's Ensight View is shown in Figure 2.
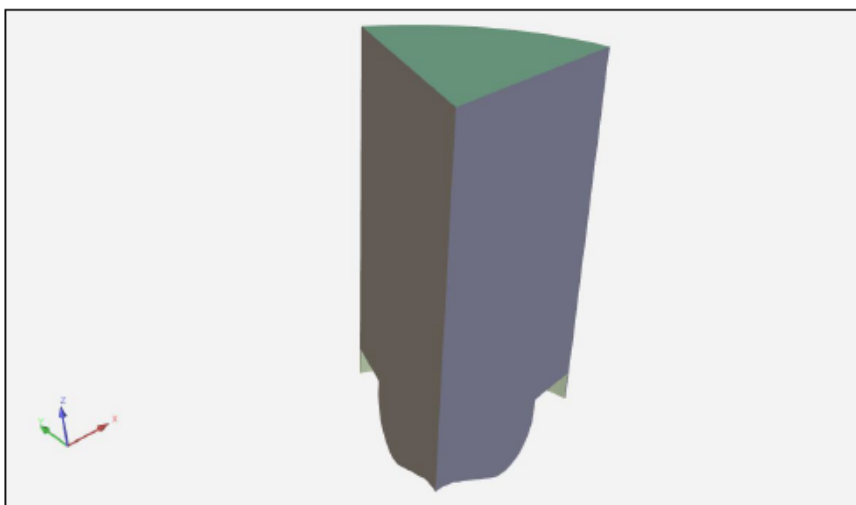

Fig. 2. Visualisation of the sector mesh geometry in Forte's Ensight View

2.5.2 Generating mesh

The simulation made direct use of the body-fitting mesh formatted in KIVA-3V. The body-fitted mesh allows the geometric model to automatically break down into distinct bodies and volumes, allowing the mesh to adjust to the bodies' natural deformations and allow for mesh deformation. Typically, in the meshing part, a grid independence test is carried out for a manually constructed mesh to achieve independence, meaning that increasing the mesh size refinement does not substantially alter the result. Usually, this process takes a very long period. However, the mesh independence investigation was finished rapidly because of ANSYS Forte's sophisticated solution

adaptive mesh refining characteristics. The grid generation's basic element size was established by an examination of grid independence, which yields optimal accuracy, stability and computing efficiency. The sector mesh was resolved to a fine resolution in the azimuthal direction. On the other hand, the z- and r-directions showed coarse mesh resolution. The meshing of the 3-D View of the 60-degree sector mesh is shown in Figure 3.
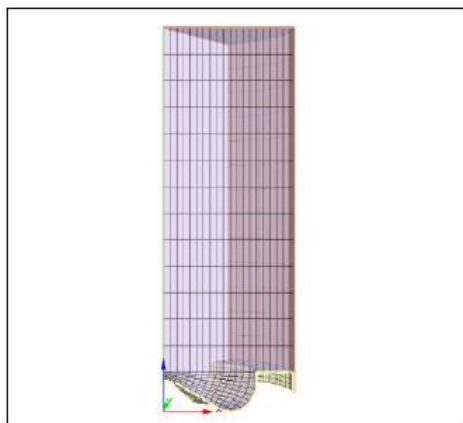

Fig. 3. Meshing of the 3-D View of the 60-degree sector mesh

2.5.3 Boundary conditions

The main four areas under boundary conditions are the piston, head, liner and injector, as shown in Figure 4. Diesel fuel is injected through a standard 0.141-millimeter diameter nozzle. In the boundary conditions section of the workflow, boundary conditions were specified in the editor panels for each of the four boundary conditions that were automatically created upon importing the mesh. The default setting for the wall model applied to all wall boundaries, was left as "Law of the Wall," with heat transfer to the wall enabled by default.

For the piston boundary condition, the piston temperature was set to 500 K and wall motion was enabled, with the motion type set to "slider crank." the following parameters were specified: stroke = 16.51, connecting rod length = 26.16 and bore = 13.716 (as pre-determined from the mesh). The option for "piston is offset" was left unchecked and the default values for the reference frame, including the global origin and direction parameters, were accepted. The defaults of x = 0.0, y = 0.0 and z = 1.0 for the piston motion direction were also retained. The default sector angle of 60 degrees was retained for the periodicity boundary condition. The periodic boundaries, periodic A and periodic B, were automatically assigned based on the boundary flags in the imported mesh. For the head boundary condition, the head temperature was set to 500 K and the changes were applied. Similarly, for the liner boundary condition, the liner temperature was set to 430 K.
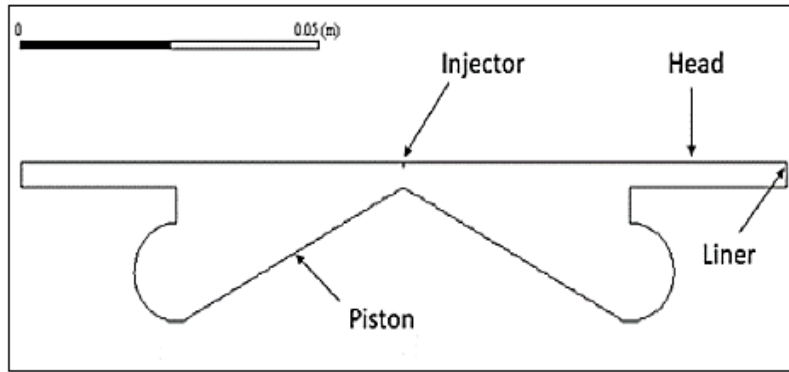
Fig. 4. Four main regions under boundary conditions

2.5.4 Combustion modelling

Turbulence investigation was performed using the RNG k-ε model. Apart from that, a pre-installed chemistry set is included with Forte employed in the chemistry model [24]. This chemistry-set file (.cks) is a conventional CHEMKIN file with a simplified system designed for dual-fuel settings. Forte's automatic time step control method calculated the actual local time steps required to perform the simulation.

For the injection of the diesel, the solid-cone spray model with droplet breakup was employed for spray injection governed by KH-RT sub-models. There are two ways to initialise the spray for solid-cone injections: using a nozzle-flow model to predict the properties of the nozzle discharge or using an empirical nozzle discharge coefficient [3]. The nozzle flow model describes these choices, which is based on Eq. (11):

$$tan\left(\frac{\theta}{2}\right) = \frac{4\pi}{A} \cdot \sqrt{\frac{\rho_g}{\rho_l}} \cdot f(T) \tag{11}$$

where A is 3+0.28(L/D), L/D is the length-to-diameter ratio of the nozzle, ρ_l is liquid fuel density and ρ_g is gas-mixture density. The function $f(T)$ is approximated by:

$$f(T) = \frac{\sqrt{3}}{6} \cdot [1 - exp(-10 \cdot T)], where\ T = \left(\frac{Re}{We}\right)^2 \cdot \frac{\rho_l}{\rho_g} \tag{12}$$

The spray atomization and droplet breakup of solid-cone sprays are modelled by the Kelvin-Helmholtz / Rayleigh-Taylor (KH /RT) hybrid breakup model [3]. Figure 5 shows the KH/RT breakdown model for solid-cone sprays and outlines the methodology for using the models. Within a given Breakup Length, L, from the nozzle outlet (region A), the KH breakup model is employed. The parent parcels or "blobs," are the tiny droplets of the jet that are removed, while the jet itself remains a dense liquid core. The RT model and the KH model are used to predict secondary break-up beyond the Breakup Length, which is in region B [3]. The rate equation is defined as:

$$\frac{r_p - r_c}{\tau_{KH}} \tag{13}$$

with

$$r_p = \frac{\Lambda_{KH}\left(1+0.87We_g^{1.67}\right)^{0.6}}{9.02(1+0.45Z^{0.5})(1+0.4T^{0.7})} \tag{14}$$

$$r_c = B_{KH}\Lambda_{KH} \tag{15}$$

$$\tau_{KH} = \frac{3.726C_{KH}r_p}{\Lambda_{KH}\Omega_{KH}} \tag{16}$$

where Λ_{KH} is the wavelength of the fastest-growing wave, Ω_{KH} is its growth rate, r_p is the jet radius, B_{KH} is the size constant of the KH breakup model, We_g is the dimensionless gas Weber number, Z is the dimensionless Ohnesorge number and *T* is the dimensionless Taylor number.

For spray injection, the Radius-of-Influence (ROI) collision model was also utilised. In ANSYS Forte, the mesh-size dependency and the time-step reliance for the droplet collision process are eliminated by the use of the ROI collision model [3]. According to the ROI approach, a particle can only collide with another if it is inside the other's radius of influence. Within a "sphere of influence" centred around the parcel's location, collision partners associated with that particular parcel are sought after [3]. Every parcel in this sphere has the potential to collide with the centre parcel through collision partners. With this method, there is no longer any reliance on the size of the collision mesh (should a separate collision mesh be employed) or the CFD mesh.

The vaporization properties for each surrogate component are also taken into account using a discrete multi-component spray-vaporization model. Spray droplet vaporisation is represented using a discrete multi-component (DMC) fuel-vaporization model in ANSYS Forte [3]. The DMC vaporisation model permits connection with the reaction kinetics of the individual fuel components and follows the individual constituents (molecules) of a real surrogate fuel during the evaporation process [3]. An explicit form of the DMC model's equation defining the heat flux from the surrounding gas mixture to the droplet-gas interface is obtained by approximating the solution of the quasi-steady energy equation. The model is made to track each fuel component regardless of the direction of the process, that is, whether evaporation off the droplet surface or condensation into the droplet is occurring [3]. For the models mentioned, the default parameters were used. An operator splitting method is utilised in conjunction with CFD simulations to solve all chemical species equations included in the comprehensive kinetic mechanism.
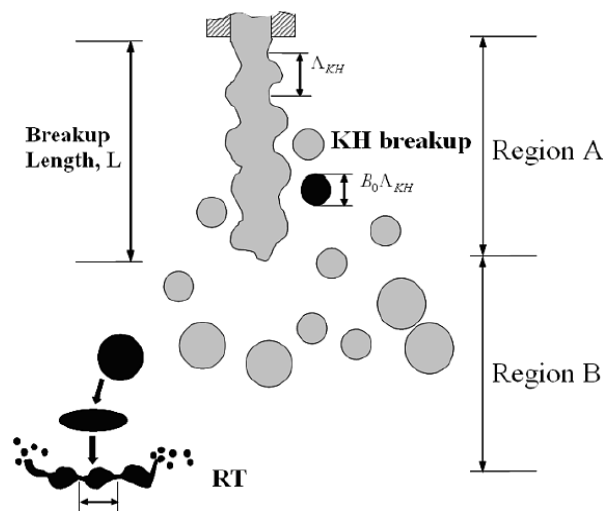

Fig. 5. The KH/RT breakdown model for solid-cone sprays outlines the methodology for using the KH/RT breakup models

2.5.5 Initialisation setup

The initialisation setup of the simulation involves determining the gas mixture composition. To determine the gas mixture composition, the premixed mass fraction of the gas mixture composition needs to be calculated using the IVC calculator in ANSYS Forte's Utility. The premixed mass fraction of the gas mixture is calculated based on the properties of diesel, the mole fraction of diesel, the mole fraction of species in reformed biogas, the mass flow rate of diesel, the mass flow rate of reformed biogas and the equivalence ratio of fuel. Once the gas mixture composition is completed, the initial condition parameters such as initial temperature, initial pressure, turbulence intensity, engine swirl and length scale are set based on this research analysis. The initial temperature and pressure conditions are fixed at 350K and 9 bar for analysing the effects of reformed biogas substitution ratio and air-fuel ratio on the performance and emission characteristics of the dual-fuel engine. On the other hand, the initial pressure condition is fixed at 9 bars for analysing the effect of reformed biogas substitution ratio with differences in inlet temperature on performance and emission characteristics. The figures below show the initialization setup for the simulation.

### 2.5.6 Simulation analysis

The combustion properties of the engine will be analysed through heat transfer using the ANSYS Forte simulation. This analysis will yield contour results for different biogas-diesel mass flow rates for several combustion characteristics, including peak pressure and the distribution of in-cylinder temperature. Results of this investigation will also be obtained for indicated mean effective pressure (IMEP), indicated gross power, thermal efficiency and combustion efficiency at various primary and pilot fuel compositions. The investigation will also showcase the outcomes of the emission performance such as emission index of nitrogen oxide (EINOx), emission of carbon oxide at the exhaust valve opening and unburnt hydrocarbon at the exhaust valve opening. Concerning each component species, this CFD model also solves conservation equations that include convection, diffusion and reaction sources. Since diesel fuel has a cetane number similar to that of petrol, diesel's liquid phase is represented by n-dodecane. Thus, the final objective of this CFD simulation is to examine how various compositions of biogas and diesel affect combustion characteristics both at constant intake temperature and air-fuel ratio and at varying inlet temperature and air-fuel ratio.

2.6 Model Validation

In this study, the developed engine sub-model should be accurate by referring to the experimental data obtained by Jagadish *et al.,* [17] to verify the accuracy of the simulation model. The effectiveness is first evaluated under traditional diesel combustion conditions with a global equivalence ratio of 1. Secondly, evaluate in the RCCI combustion setting of reformed biogas diesel with a constant global equivalence ratio of 1.00. To evaluate the effectiveness of this multi-fuel system, reformed biogas replaced 20%, 40% and 60% of the total input energy. The results are consistent with the experimental results.

In all situations, the composition of reformed biogas was 53.1% nitrogen, 10.6% water, 1.87% carbon dioxide, 20.6% hydrogen and 13.8% carbon monoxide (by volume). The total input energy of the engine remained constant at 5100 J/cycle during validation and subsequent simulations. Figure 5 shows the experimental and numerical comparison of cylinder pressure under traditional diesel mode with an equivalence ratio of 1.00. The simulation model accurately predicted cylinder pressure over a wide range of equivalence ratios. Similar to the traditional diesel situation, this model can

represent the combustion characteristics within the studied substitution ratio range. All simulation diagrams indicate that the current model has been successfully generated and may exhibit behaviour comparable to that of the experimental engine.
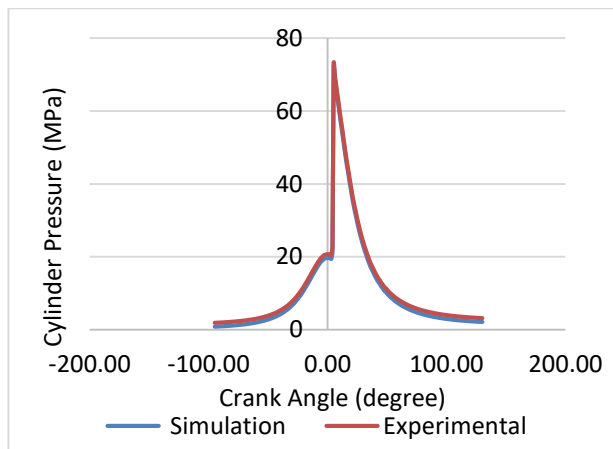
(a) Cylinder pressure (MPa) against crank angle for 20% reformed biogas substitution
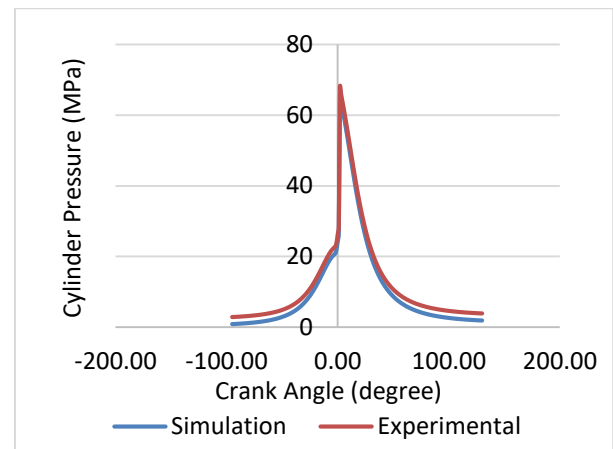
(b) Cylinder pressure (MPa) against crank angle for 40% reformed biogas substitution
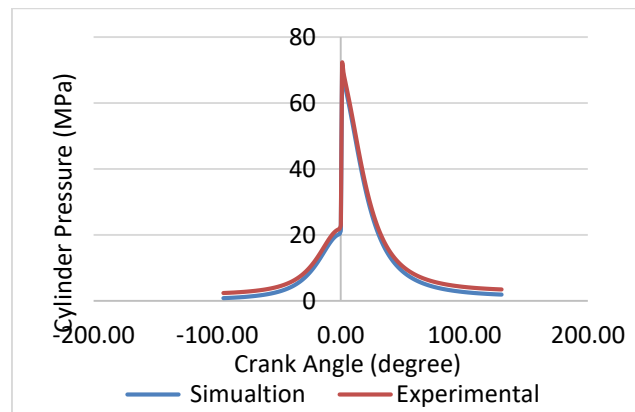
(c) Cylinder pressure (MPa) against crank angle for 60% reformed biogas substitution

Fig. 5. Comparisons of the cylinder pressure between numerical and experiments with varying substitution ratios of reformed biogas under 1300 rpm mid-load

3. Results

3.1 Effect of Reformed Biogas Substitution Ratio on Performance of Dual-Fuel Engine

The global equivalency ratio, which is equal to 1 and 5100 J/cycle of the total energy input given to the engine are both regarded as constants per cycle. Also, the inlet pressure, which is 9 bar, is regarded as constant per cycle. The result of the reformed biogas substitution ratio on the performance of the dual-fuel engine is tabulated in Table 5.

Table 5
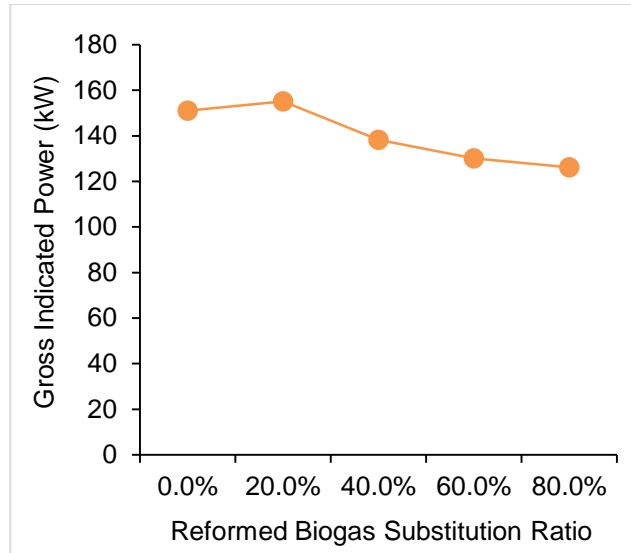Result of the reformed biogas substitution ratio on the performance of the dual-fuel engine

Reformed biogas substitution (%)	Indicated mean effective pressure (MPa)	Gross indicated power (kW)	Combustion efficiency	Thermal efficiency
0.0	5.715	151.035	0.932	0.347
20.0	5.871	155.156	0.965	0.366
40.0	5.233	138.290	1.000	0.408
60.0	4.924	130.134	1.000	0.485
80.0	0.061	1.614	0.395	0.100

Figure 6 shows how substituting gaseous fuel, such as reformed biogas, a low reactivity fuel, for diesel fuel in the intake stroke will cause the gaseous fuel to displace some of the input air and reduce volumetric efficiency. The dual-fuelled engine will perform less well than the conventional diesel combustion engine due to a drop in indicated mean effective pressure (IMEP) and indicated gross power (IGP), as shown in Figure 6(a) and Figure 6(b). On the other hand, Figure 6(c) depicts the thermal efficiency of dual-fuelled engines revealing a steady increase over the reformed biogas substitution, however, it significantly reduces with 79.4% at 80% of reformed biogas substitution compared to 60% of reformed biogas substitution. Additionally, the combustion efficiency of dual-fuelled engines unveils a steady increase over the reformed biogas substitution, however, it significantly reduces with 60.5% at 80% of reformed biogas substitution compared to 60% of reformed biogas substitution, as illustrated in Figure 6(d).

In addition, due to the easy formation of a uniform mixture between reformed biogas and air, combustion occurs almost simultaneously throughout the room, which explains the slight increase in thermal and combustion efficiency of reformed biogas as a substitute compared to controlled diffusion combustion (CDC) mode [21]. In addition, injecting a small amount of diesel (an ignition fuel) may cause strong combustion. On the contrary, in the case of 80% reformed biogas substitution, it is believed that high concentrations of nitrogen and water vapour in the premixed charge will lower the average gas temperature of the cylinder, leading to a significant decrease in thermal efficiency and combustion efficiency [9,21]. When the substitution rate of reformed biogas changes, all scenarios show a decrease in working output. The global equivalence ratio can be seen as decreasing proportionally to the increase in the energy share of gaseous fuels to offset the decrease in workload. In this case, using reformed biogas can reduce emissions while maintaining output power at medium or even higher loads.
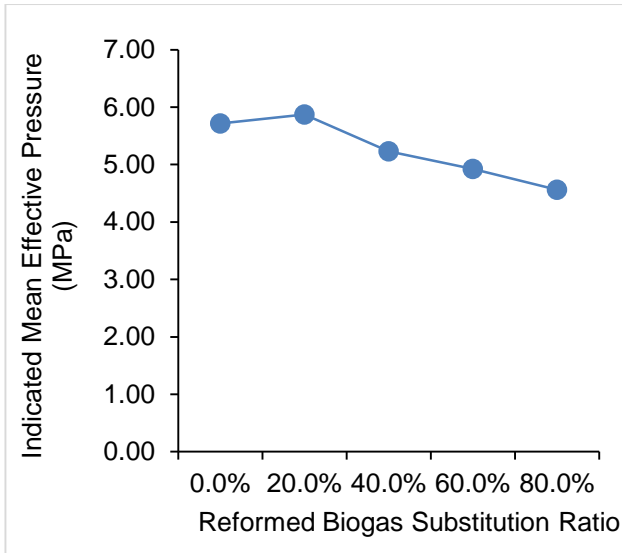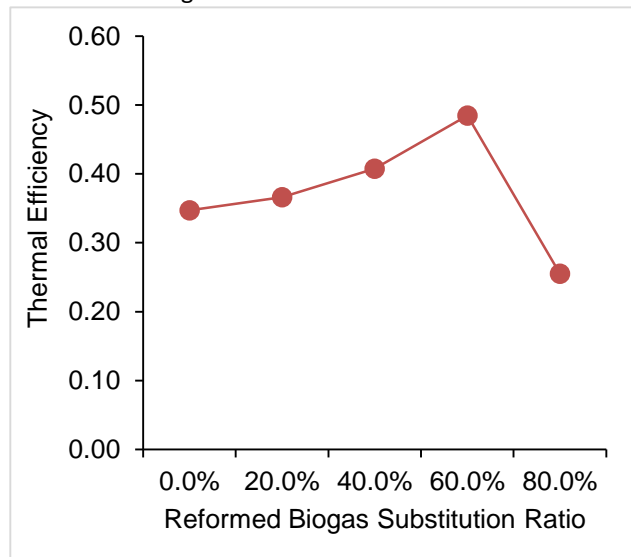
(a) Indicated mean effective pressure against substitution ratio of reformed biogas

(b) Gross indicated power (kW) against substitution ratio of reformed biogas
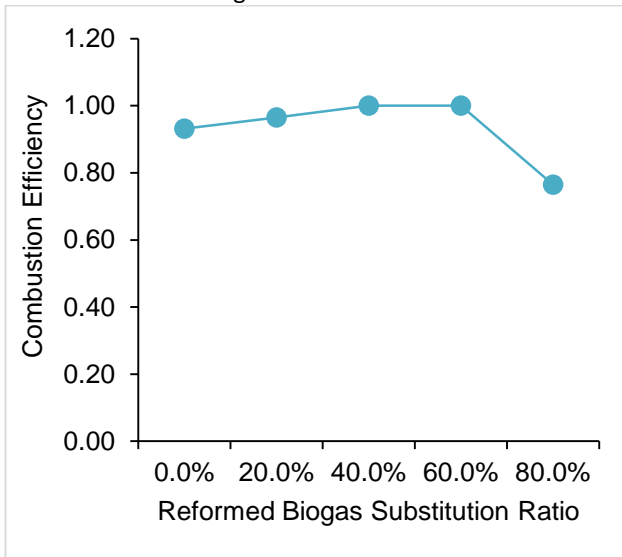
(c) Combustion efficiency against substitution ratio of reformed biogas

(d) Thermal efficiency against substitution ratio of reformed biogas

Fig. 6. Effect of reformed biogas on the (a) Indicated mean effective pressure (b) Gross indicated power (c) Combustion efficiency (d) Thermal efficiency

3.2 Effect of Reformed Biogas Substitution Ratio on Emissions

Unburned hydrocarbons (UHC), carbon monoxide (CO) and nitrogen oxides (NOx) are the three main pollutants from internal combustion engines that have an impact on engine performance. The present investigation employs the special emission (SE) approach, which is expressed in g/kW.hr, to quantify the concentration of these pollutants. Apart from that, the nitrogen in the premixed charge (air-gaseous fuel mixture) is primarily responsible for the NOx emission level. Nitrogen is a stable diatomic molecule at low temperatures; nonetheless, beyond 1800 K, it breaks down into monatomic nitrogen N, which interacts with oxygen to form a reaction [21]. The result of the reformed biogas substitution ratio on the emissions of the dual-fuel engine is tabulated in Table 6. The lower combustion temperature of reformed biogas-diesel results in a lower NO_x emission level as shown in Figure 7(a). It was found that the emission index of nitrogen oxide at the exhaust valve opening rose

gradually as the reformed biogas substitution ratio increased, nevertheless, the emission index of nitrogen oxide decreased by 24.8% at 80% of reformed biogas substitution compared to 60% of reformed biogas substitution. As opposed to using dodecane in the pure diesel mode, using 60% reformed biogas substitution in the dual-fuel mode reduces NO_x emissions by as much as 70%. The low temperature of reformed biogas-diesel combustion, which results from a lean reformed biogas-air mixture from the initial CO_2 and water vapour concentrations, is the cause of the low NO_x generation [21]. When there is a shortage of fuel, replacing a greater amount of diesel with reformed biogas results in a significant decrease in NO_x emissions.

Table 6
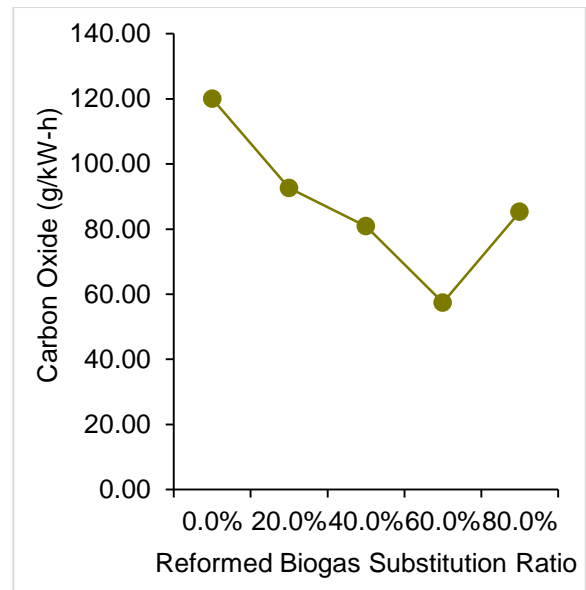Result of the reformed biogas substitution ratio on the emissions of the dual-fuel engine

Reformed biogas substitution (%)	Emission index nitrogen oxide (NO_x) at exhaust valve opening (g/kW-h)	Carbon oxide (CO) at exhaust valve opening (g/kW-h)	Unburnt hydrocarbon at exhaust valve opening (g/kW-h)
0.0%	0.254	120.113	2.052
20.0%	0.444	92.604	2.117
40.0%	0.467	80.858	0.380
60.0%	0.844	57.411	0.000
80.0%	0.635	85.300	0.980

Figure 7(b) shows the variation of CO emission at the exhaust valve opening versus the reformed biogas substitution ratio. It was discovered that the CO emission at the exhaust valve opening fell steadily along the reformed biogas substitution, however, the CO emission rose about 32.7% at 80% of the reformed biogas substitution compared to 60% of the reformed biogas substitution. Moreover, when 80% reformed biogas substitution is used in the dual-fuel mode instead of dodecane, CO emissions are reduced by up to 30%. From the relationship between CO emissions when the exhaust valve is opened and the replacement ratio of reformed biogas, it can be seen that the formation of CO emissions is due to the insufficient oxygen supply in the rich oil mixture, resulting in incomplete oxidation of carbon atoms [9]. It is also caused by a lean mixture with a combustion temperature below 1450 K. The low temperature is due to the presence of water vapour in the reformed biogas, which increases CO emissions, while NOx emissions are relatively low compared to the CDC mode [9]. Therefore, by increasing the replacement ratio of reformed biogas, the CO level will significantly increase. This will lead to a shortage of oxygen in the cylinder and an increase in the hydrogen-carbon ratio. On the other hand, an increase in the concentration of reformed biogas in the intake leads to a shortened combustion time, thereby reducing the opportunity to convert CO_2 into CO.

Furthermore, Figure 7(c) represents that as the substitution percentage increases, the unburned hydrocarbons released from reforming biogas diesel combustion will be significantly reduced. However, the UHC replaced by 80% reforming biogas increases by up to 99% compared to the UHC replaced by 60% reforming biogas. This is due to the increase in average gas temperature in the cylinder, especially the local high temperature in the combustion chamber, which enhances the reactivity of these areas, causing the flame to burn to the inner lining. On the contrary, in the combustion of reformed biogas diesel, due to the presence of CO_2 and H_2O, a low-temperature zone is formed, so the flame may extinguish earlier [9]. In this case, some liquid fuel (diesel) particles will penetrate the gap between the piston and cylinder wall after hitting the cylinder wall and then remain unburned at the end of combustion.
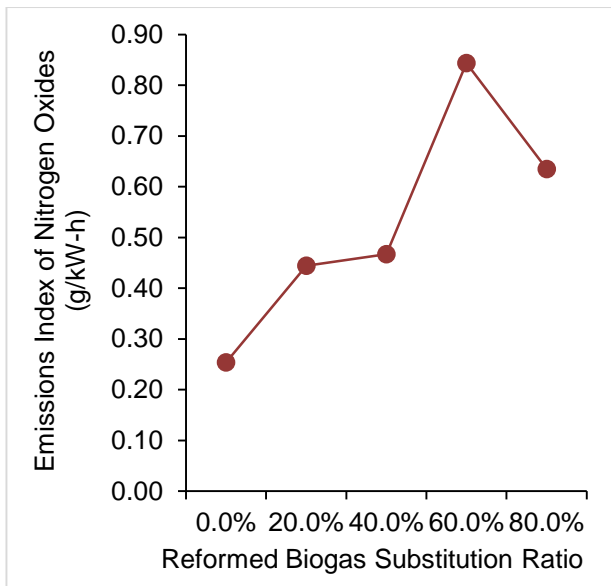
(a) Emission index NOx at exhaust valve opening against substitution ratio of reformed biogas

(b) Carbon oxide at exhaust valve opening against substitution ratio of reformed biogas
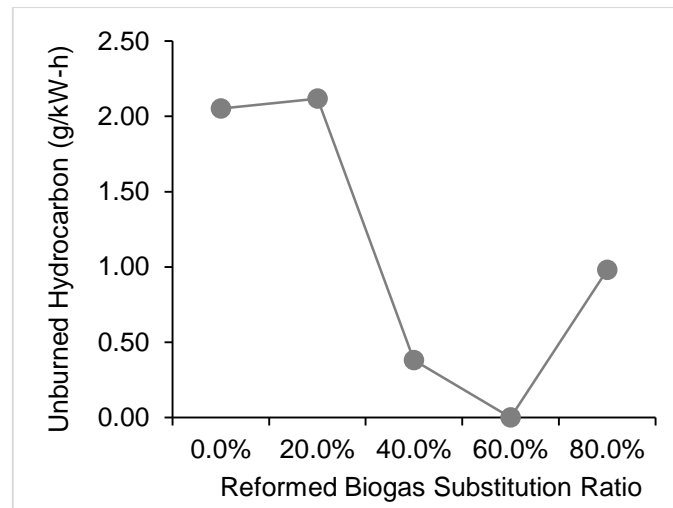
(c) Unburnt hydrocarbon at exhaust valve opening against substitution ratio of reformed biogas

Fig. 7. Effect of reformed biogas on the (a) Emission index NO_x (b) Carbon oxide (c) Unburnt hydrocarbon at exhaust valves opening

3.3 Effect of Reformed Biogas Substitution Ratio with Differences of Inlet Temperature on the Performance of Dual-Fuel Engine

Both the overall energy input provided to the engine and the global equivalency ratio, which is equal to 1 and 5100 J/cycle, are thought of as constants per cycle. The inlet pressure, which is 9 bar, also is regarded as constant per cycle. Table 7 tabulates the effect of the reformed biogas replacement ratio on the dual-fuel engine's performance with varying inlet temperatures. Figure 8 depicts the effect of the reformed biogas substitution ratio with differences in inlet temperature on the performance of the dual-fuelled engine.

Table 7
Result of the reformed biogas replacement ratio on the dual-fuel engine's performance with varying inlet temperatures
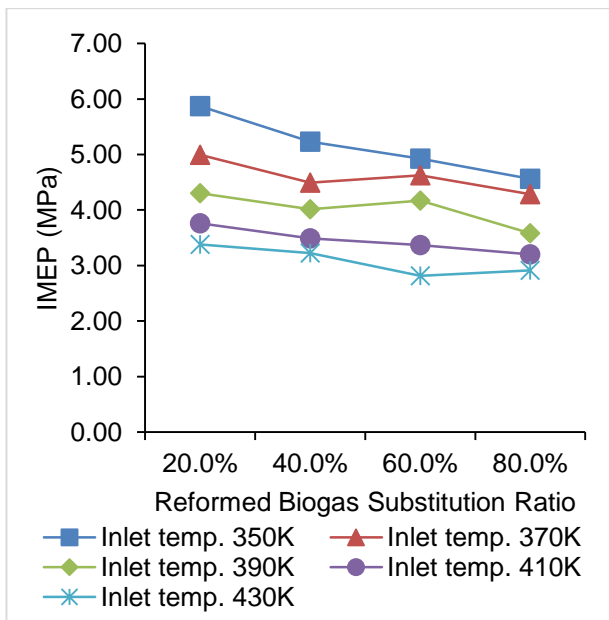
Inlet temperature - 350K; Inlet pressure - 9 bar; Air-fuel ratio - 1.00				
Reformed biogas substitution (%)	Indicated mean effective pressure (MPa)	Gross indicated power (kW)	Combustion efficiency	Thermal efficiency
0.0%	5.715	151.035	0.932	0.347
20.0%	5.871	155.156	0.965	0.366
40.0%	5.233	138.290	1.000	0.408
60.0%	4.924	130.134	1.000	0.485
80.0%	4.561	126.136	0.765	0.255
Inlet temperature - 370K; Inlet pressure - 9 bar; Air-fuel ratio - 1.00				
Reformed biogas substitution (%)	Indicated mean effective pressure (MPa)	Gross indicated power (kW)	Combustion efficiency	Thermal efficiency
20.0%	4.998	132.076	0.955	0.327
40.0%	4.491	118.683	1.000	0.368
60.0%	4.628	122.314	1.000	0.479
80.0%	4.283	113.186	1.000	0.574
Inlet temperature - 390K; Inlet pressure - 9 bar; Air-fuel ratio - 1.00				
Reformed biogas substitution (%)	Indicated mean effective pressure (MPa)	Gross indicated power (kW)	Combustion efficiency	Thermal efficiency
20.0%	4.305	113.775	0.947	0.295
40.0%	4.014	106.081	1.000	0.344
60.0%	4.171	110.238	1.000	0.453
80.0%	3.580	94.616	1.000	0.504
Inlet temperature - 410K; Inlet pressure - 9 bar; Air-fuel ratio - 1.00				
Reformed biogas substitution (%)	Indicated mean effective pressure (MPa)	Gross indicated power (kW)	Combustion efficiency	Thermal efficiency
20.0%	3.760	99.378	0.939	0.270
40.0%	3.491	92.245	1.000	0.313
60.0%	3.367	88.979	1.000	0.383
80.0%	3.201	84.593	1.000	0.473
Inlet temperature - 430K; Inlet pressure - 9 bar; Air-fuel ratio - 1.00				
Reformed biogas substitution (%)	Indicated mean effective pressure (MPa)	Gross indicated power (kW)	Combustion efficiency	Thermal efficiency
20.0%	3.381	89.348	0.931	0.253
40.0%	3.222	85.161	1.000	0.301
60.0%	2.815	74.396	1.000	0.334
80.0%	2.915	77.029	1.000	0.450

The IMEP decreased with increasing reformed biogas substitution across all inlet temperatures in Figure 8(a). For example, at 350K, the IMEP dropped from 5.715 MPa at 0% substitution to 4.561 MPa at 80%. This trend was consistent across higher inlet temperatures, indicating a general decline in IMEP with both higher biogas substitution and temperature [12]. This decrease can be attributed to the lower calorific value of biogas, which provides less energy per unit volume compared to conventional fuels and the higher carbon dioxide content in biogas, which acts as an inert component, diluting the air-fuel mixture and reducing combustion efficiency.

Moreover, the gross indicated power showed a similar downward trend with increasing biogas substitution ratios, as depicted in Figure 8(b). At 350K, the power decreased from 151.035 kW at 0% to 126.136 kW at 80% substitution. Higher inlet temperatures exacerbated this decline; for instance, at 430K, power dropped from 89.348 kW at 20% to 77.029 kW at 80%. This reduction in power output is due to the lower energy density of biogas, leading to less energy being available for conversion into mechanical work and the altered heat release rate during biogas combustion, which affects the overall power output, especially at higher substitution levels [7].

Apart from that, the combustion efficiency remained relatively stable across different biogas substitution ratios, as shown in Figure 8(c). At 350K, the efficiency was highest at 40-60% substitution ratios, reaching 1.00, but it decreased to 0.765 at 80% substitution. This stability was observed across other temperatures, indicating that combustion efficiency is less sensitive to biogas substitution but still affected by it. This stability was observed across other temperatures, indicating that combustion efficiency is less sensitive to biogas substitution but still affected by it [7]. The stability at moderate substitution ratios suggests that biogas can achieve relatively complete combustion when properly mixed and ignited. However, very high substitution ratios lead to a drop in efficiency due to increased dilution and lower flame temperatures, which impede complete combustion [7].

Furthermore, the thermal efficiency, illustrated in Figure 8(d), generally increased with higher biogas substitution up to a certain point before declining. At 350K, thermal efficiency rose from 0.347 at 0% substitution to 0.485 at 60%, before dropping at 80%. Higher temperatures showed a similar pattern, suggesting an optimal substitution range for maximizing thermal efficiency. Higher temperatures showed a similar pattern, suggesting an optimal substitution range for maximizing thermal efficiency. This increase in efficiency at moderate substitution levels is likely due to the optimal air-fuel mixture that enhances combustion, while the presence of CO_2 in biogas helps moderate combustion temperatures and reduce heat losses [14]. However, beyond 60% substitution, the dilution effect of CO_2 outweighs its benefits, leading to a decrease in thermal efficiency due to incomplete combustion.

(a) Indicated mean effective pressure against substitution ratio of reformed biogas
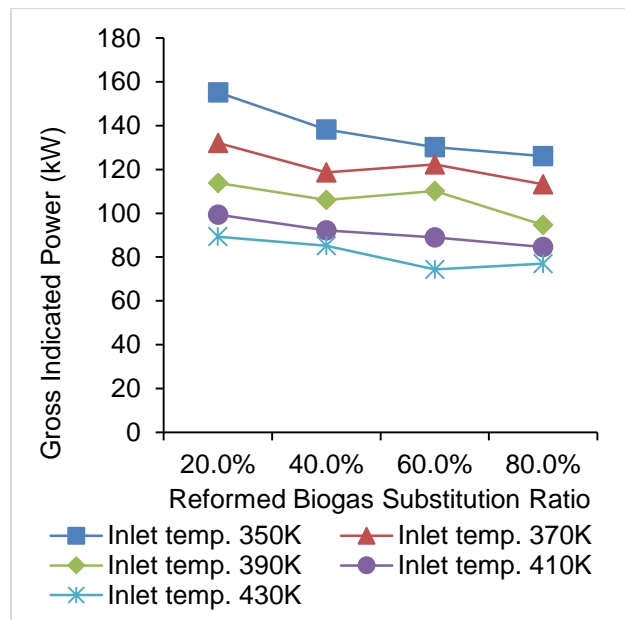
(b) Gross indicated power against substitution ratio of reformed biogas
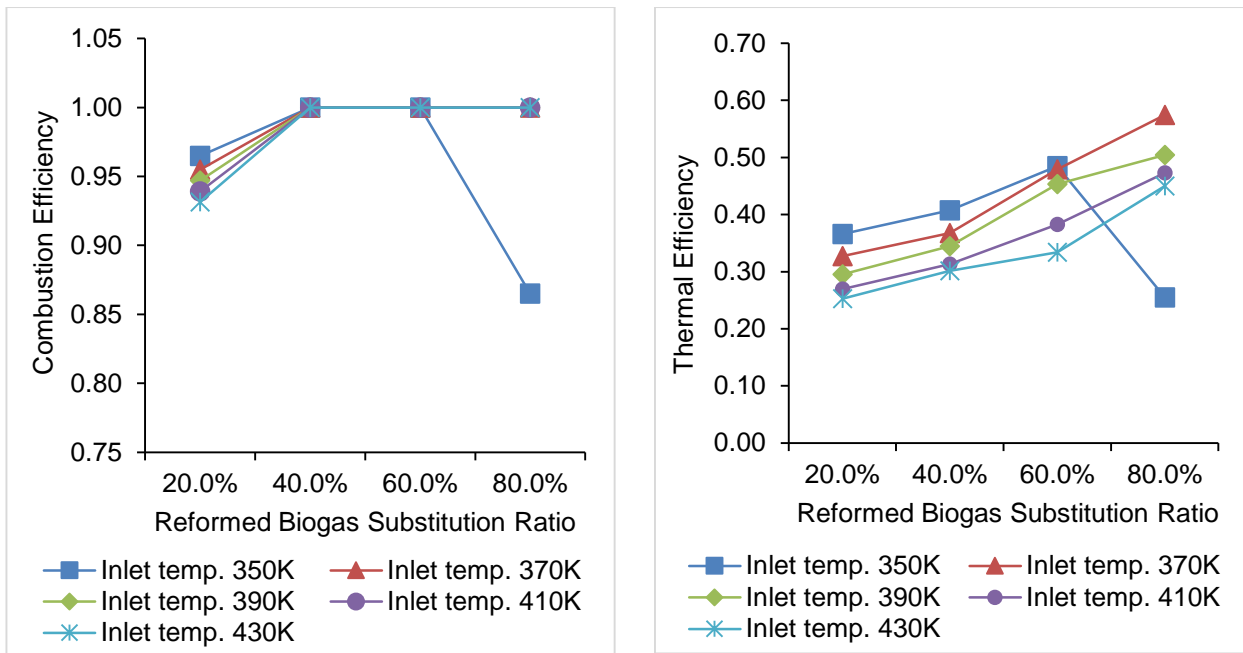
(c) Combustion efficiency against substitution ratio of reformed biogas

(d) Thermal efficiency against substitution ratio of reformed biogas

Fig. 8. Impact of reformed biogas on the (a) Indicated mean effective pressure (b) Gross indicated power (c) Combustion efficiency (d) Thermal efficiency with varying inlet temperatures

3.4 Effect of Reformed Biogas Substitution Ratio with Differences of Inlet Temperature on Emissions

Similar to the previous sub-chapter of 3.3, the global equivalency ratio, which is equivalent to 1 and 5100 J/cycle and the total energy input supplied to the engine are both considered to be constants per cycle. Additionally, the 9-bar inlet pressure is thought to be constant throughout each cycle. The emission characteristics of the dual-fuel engine, influenced by reformed biogas substitution and inlet temperature, reflect the complex interactions between combustion dynamics and fuel properties.

Table 8 and Figure 9 demonstrate the impact of reformed biogas substitution and inlet temperature on emissions. The emission index for nitrogen oxides (NOx) generally increased with higher biogas substitution and inlet temperatures, as seen in Figure 9(a). At 350K, NOx emissions rose from 0.444 g/kW-h at 20% to 0.635 g/kW-h at 80%. This increase was more pronounced at higher temperatures, with NOx emissions at 430K rising from 0.365 g/kW-h at 20% to 1.324 g/kW-h at 80%. This trend can be explained by the thermal NOx formation mechanism, which is highly sensitive to combustion temperature. As the inlet temperature rises, the peak combustion temperatures increase, leading to more significant NOx formation [14]. Additionally, while biogas contains a considerable amount of CO_2, which can help moderate combustion temperatures and reduce NOx formation at lower substitution ratios, the overall lower energy content and increased dilution effect at higher substitution ratios can cause incomplete combustion [12]. This incomplete combustion can result in localized hot spots where NOx formation is enhanced.

Carbon monoxide (CO) emissions showed a decreasing trend with higher biogas substitution and inlet temperatures, as shown in Figure 9(b). At 350K, CO emissions dropped from 92.604 g/kW-h at 20% to 85.300 g/kW-h at 80%. The reduction was more significant at higher temperatures, with CO emissions at 430K declining from 178.269 g/kW-h at 20% to 48.156 g/kW-h at 80%. This decrease can be attributed to the enhanced combustion process facilitated by the higher CO2 content in biogas, which acts as a thermal buffer, improving the combustion efficiency by reducing the peak

temperatures and promoting more complete oxidation of CO [7]. The higher temperatures contribute to more efficient combustion, thereby reducing CO emissions as the biogas substitution ratio increases.

Table 8
Result of the reformed biogas replacement ratio on emission with varying inlet temperatures

| Inlet temperature - 350K; Inlet pressure - 9 bar; Air-fuel ratio - 1.00			
Reformed biogas substitution (%)	Emission index nitrogen oxide (NO_x) at exhaust valve opening (g/kW-h)	Carbon oxide at exhaust valve opening (g/kW-h)	Unburnt hydrocarbon at exhaust valve opening (g/kW-h)
20.0%	0.444	92.604	2.117450
40.0%	0.467	80.858	0.380466
60.0%	0.844	57.411	0.000118
80.0%	0.635	85.300	0.980000
Inlet temperature - 370K; Inlet pressure - 9 bar; Air-fuel ratio - 1.00			
Reformed biogas substitution (%)	Emission index nitrogen oxide (NO_x) at exhaust valve opening (g/kW-h)	Carbon oxide at exhaust valve opening (g/kW-h)	Unburnt hydrocarbon at exhaust valve opening (g/kW-h)
20.0%	0.269	117.533	0.052004
40.0%	0.381	96.447	0.002305
60.0%	0.888	61.350	0.002285
80.0%	1.425	33.156	0.000405
Inlet temperature - 390K; Inlet pressure - 9 bar; Air-fuel ratio - 1.00			
Reformed biogas substitution (%)	Emission index nitrogen oxide (NO_x) at exhaust valve opening (g/kW-h)	Carbon oxide at exhaust valve opening (g/kW-h)	Unburnt hydrocarbon at exhaust valve opening (g/kW-h)
20.0%	0.267	137.963	0.000168
40.0%	0.450	108.874	0.000231
60.0%	1.052	67.969	0.000323
80.0%	1.238	38.854	0.000012
Inlet temperature - 410K; Inlet pressure - 9 bar; Air-fuel ratio - 1.00			
Reformed biogas substitution (%)	Emission index nitrogen oxide (NO_x) at exhaust valve opening (g/kW-h)	Carbon oxide at exhaust valve opening (g/kW-h)	Unburnt hydrocarbon at exhaust valve opening (g/kW-h)
20.0%	0.312	159.385	0.000231
40.0%	0.449	124.988	0.000127
60.0%	0.695	83.797	0.001444
80.0%	1.267	43.569	0.000021
Inlet temperature - 430K; Inlet pressure - 9 bar; Air-fuel ratio - 1.00			
Reformed biogas substitution (%)	Emission index nitrogen oxide (NO_x) at exhaust valve opening (g/kW-h)	Carbon oxide at exhaust valve opening (g/kW-h)	Unburnt hydrocarbon at exhaust valve opening (g/kW-h)
20.0%	0.365	178.269	0.000252
40.0%	0.573	136.257	0.000096
60.0%	0.669	100.596	0.001272
80.0%	1.324	48.156	0.000023

UHC emissions decreased with increasing biogas substitution, particularly at higher temperatures, as depicted in Figure 9(c). This trend can be explained by the presence of CO_2 in biogas, which enhances the combustion process by acting as a diluent and thermal moderator. At lower biogas substitution ratios, the combustion process might not be as efficient, leading to higher UHC emissions. However, as the biogas substitution ratio increases, the improved combustion efficiency due to better thermal management leads to a reduction in UHC emissions. For example, at 350K,

UHC emissions fell from 2.117450 g/kW-h at 20% to 0.980 g/kW-h at 80%. Higher inlet temperatures further enhance this effect, resulting in even lower UHC emissions across all substitution ratios. This indicates that higher biogas substitution ratios and inlet temperatures synergistically improve the completeness of combustion, thereby reducing UHC emissions [12].
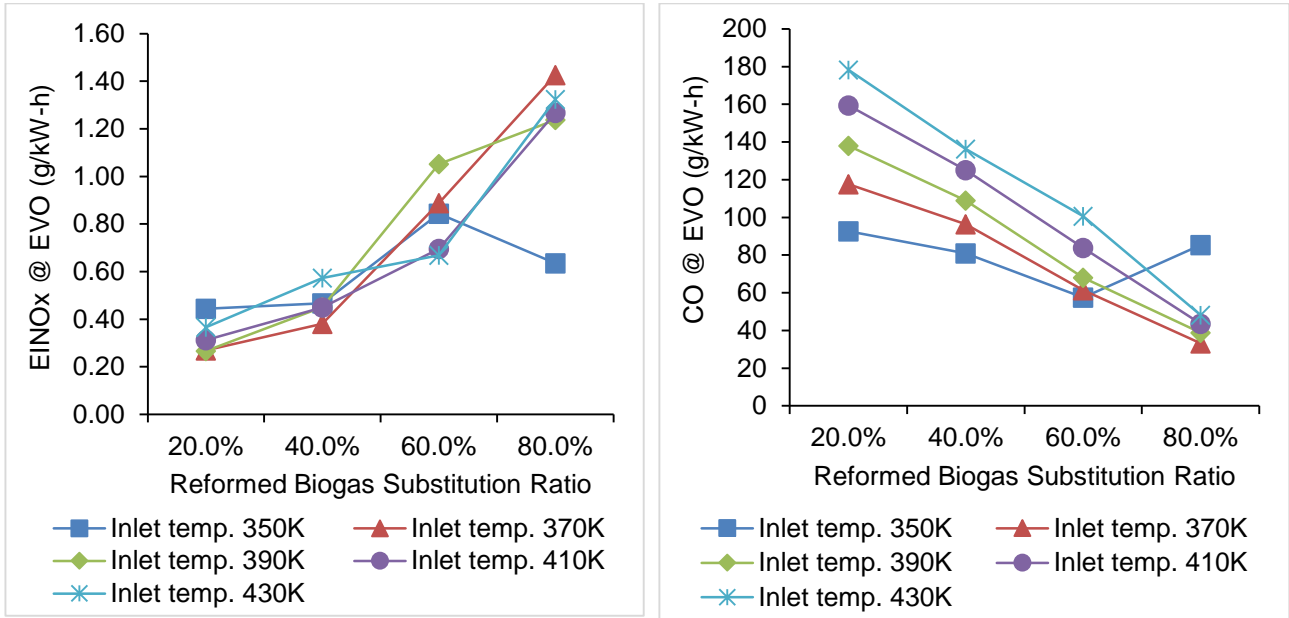
(a) Emission index of nitrogen oxide at exhaust valve opening against substitution ratio of reformed biogas

(b) Carbon oxide at exhaust valve opening against substitution ratio of reformed biogas
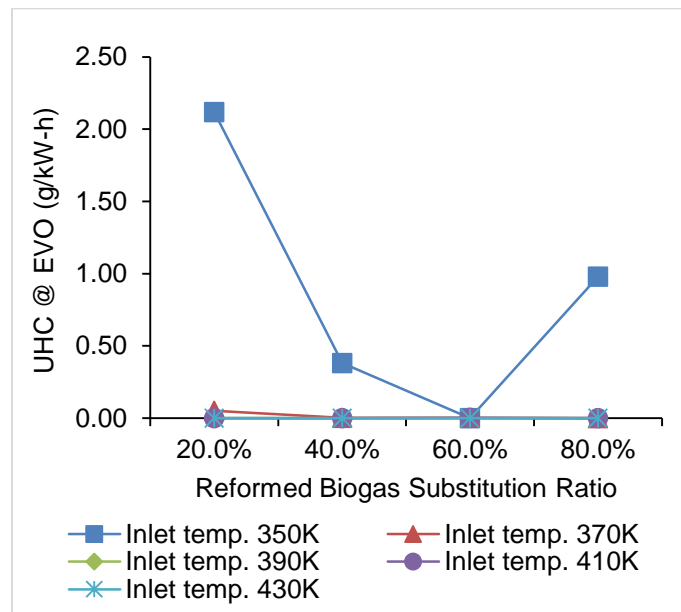
(c) Unburned hydrocarbon at exhaust valve opening against substitution ratio of reformed biogas

Fig. 9. Impact of reformed biogas on the (a) Emission index NO_x (b) Carbon oxide (c) Unburnt hydrocarbon at exhaust valves opening with varying inlet temperatures

3.5 Effect of Reformed Biogas Substitution Ratio with Differences of Equivalence Ratio on the Performance of Dual-Fuel Engine

The overall energy input given to the engine is regarded as a constant per cycle, as is the inlet temperature, which is equal to 350K and 5100 J/cycle. Furthermore, each cycle is assumed to maintain a constant 9-bar inlet pressure. The influence of reformed biogas substitution and varying air-fuel ratios on engine performance is detailed in Table 9 and Figure 10.

Table 9
Result of the reformed biogas replacement ratio on the dual-fuel engine's performance with varying air-fuel ratio

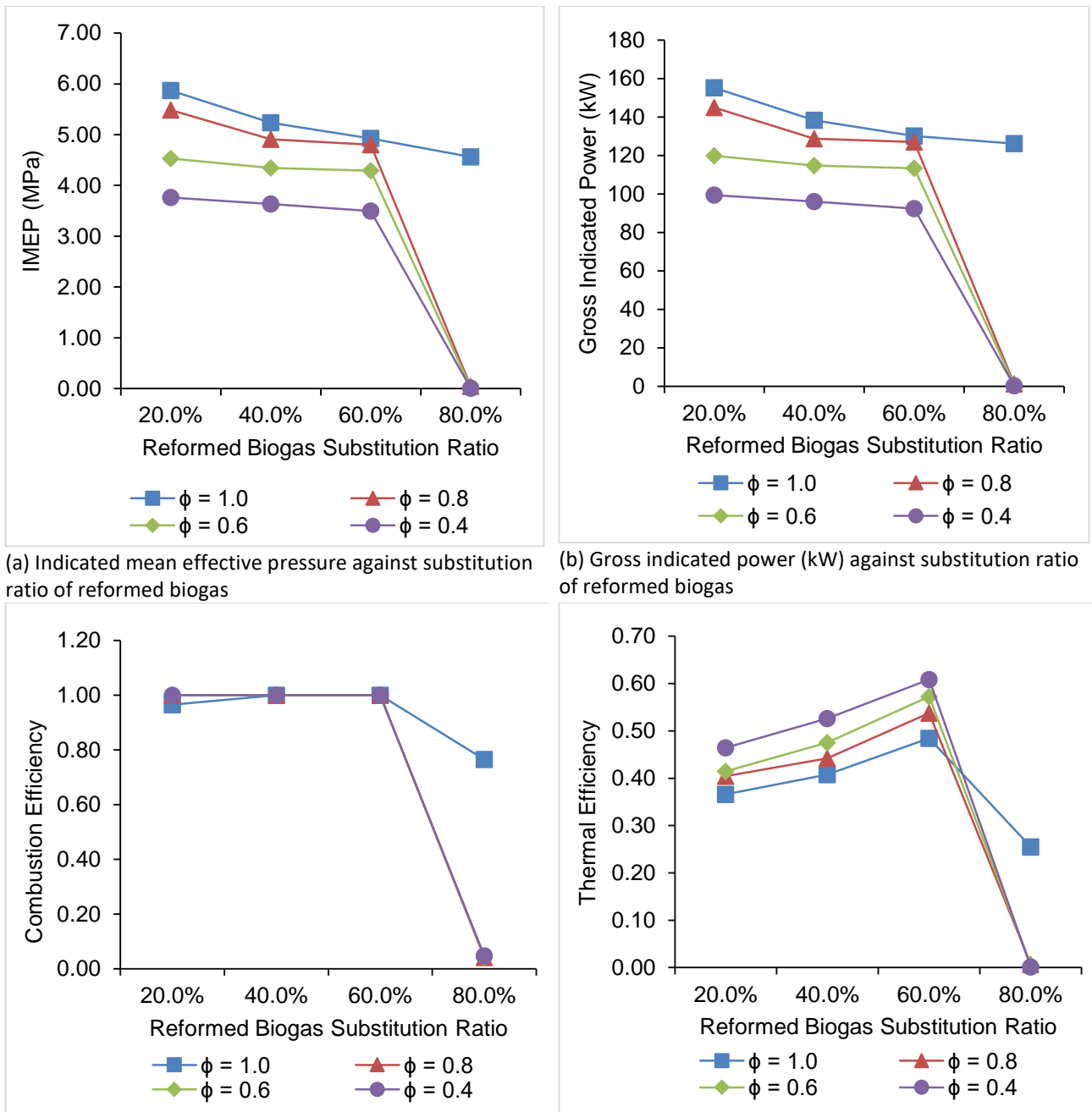| Inlet temperature - 350K; Inlet pressure - 9 bar; Air-fuel ratio - 1.00				
Reformed biogas substitution (%)	Indicated mean effective pressure (MPa)	Gross indicated power (kW)	Combustion efficiency	Thermal efficiency
0.0%	5.715	151.035	0.932	0.347
20.0%	5.871	155.156	0.965	0.366
40.0%	5.233	138.290	1.000	0.408
60.0%	4.924	130.134	1.000	0.485
80.0%	4.561	126.136	0.765	0.255
Inlet temperature - 350K; Inlet pressure - 9 bar; Air-fuel ratio - 0.80				
Reformed biogas substitution (%)	Indicated mean effective pressure (MPa)	Gross indicated power (kW)	Combustion efficiency	Thermal efficiency
20.0%	5.485	144.956	1.000	0.404
40.0%	4.910	128.683	1.000	0.442
60.0%	4.804	126.956	1.000	0.538
80.0%	0.047	1.251	0.041	0.007
Inlet temperature - 350K; Inlet pressure - 9 bar; Air-fuel ratio - 0.60				
Reformed biogas substitution (%)	Indicated mean effective pressure (MPa)	Gross indicated power (kW)	Combustion efficiency	Thermal efficiency
20.0%	4.533	119.791	1.000	0.414
40.0%	4.344	114.808	1.000	0.475
60.0%	4.289	113.344	1.000	0.573
80.0%	0.029	0.768	0.043	0.005
Inlet temperature - 350K; Inlet pressure - 9 bar; Air-fuel ratio - 0.40				
Reformed biogas substitution (%)	Indicated mean effective pressure (MPa)	Gross indicated power (kW)	Combustion efficiency	Thermal efficiency
20.0%	3.762	99.420	1.000	0.464
40.0%	3.634	96.038	1.000	0.526
60.0%	3.494	92.326	1.000	0.609
80.0%	0.006	0.162	0.047	0.001

IMEP consistently decreased with higher biogas substitution ratios across all air-fuel ratios, as shown in Figure 10(a). For example, at an air-fuel ratio (AFR) of 1.0, IMEP decreased from 5.715 MPa at 0% substitution to 4.561 MPa at 80%, which is depicted in Figure 10(a). Lower AFR values resulted in more significant reductions, with IMEP nearly dropping to zero at 80% substitution for AFR 0.4. IMEP, a measure of the average pressure in the combustion chamber, consistently decreased with higher biogas substitution ratios across all air-fuel ratios (AFR). This trend can be attributed to the lower calorific value of biogas compared to conventional fuels. Biogas has a significant number of

inert components like carbon dioxide, which do not contribute to combustion. As the proportion of biogas increases, the effective energy content of the fuel mixture decreases, leading to lower combustion pressure and, consequently, reduced IMEP [9].

Moreover, the gross indicated power also declined with higher biogas substitution ratios, as indicated in Figure 10(b). The gross indicated power, which represents the engine's ability to convert fuel energy into mechanical work, also declined with higher biogas substitution ratios. This decline is closely related to the decrease in IMEP. Based on Figure 10(b), at AFR 1.0, power decreased from 151.035 kW at 0% to 126.136 kW at 80%. The power reduction is more severe at lower AFRs, with power nearly reaching zero at 80% substitution for AFR 0.4. This drastic reduction at lower AFRs can be explained by the fact that lower AFRs result in richer fuel mixtures, when combined with high biogas substitution, leading to excessive dilution by inert gases, causing inefficient combustion and very low power output [9,21].

In addition, the combustion efficiency remained relatively high at lower biogas substitution ratios but decreased significantly at higher ratios, particularly at lower AFRs, as shown in Figure 10(c). For instance, at AFR 1.0, combustion efficiency was 1.00 at 40% substitution but dropped significantly at 80%. This indicates that at moderate substitution ratios, the combustion process is nearly complete, but at higher ratios, the increased presence of inert gases like CO_2 hinders complete combustion [14]. At AFR 0.4, efficiency remained near 1.000 up to 60% substitution but fell drastically at higher substitution ratios. The severe drop in efficiency at high substitution and low AFRs highlights the challenge of maintaining complete combustion when the fuel mixture is heavily diluted with non-combustible components [9].

Furthermore, the thermal efficiency, depicted in Figure 10(d), increased with higher biogas substitution up to a point before declining at 80%. Apart from that, thermal efficiency, which measures how well the engine converts the energy in the fuel into useful work, showed an interesting pattern. According to Figure 10(d), it increased with higher biogas substitution up to a point before declining at 80%. At AFR 1.0, thermal efficiency peaked at 0.485 at 60% substitution. This suggests that there is an optimal biogas substitution level where the combustion process is most efficient, likely due to the thermal moderation effect of CO_2, which helps control combustion temperatures and reduce heat losses [21]. However, beyond this optimal point, the efficiency drops as the negative effects of fuel dilution and incomplete combustion become more pronounced. Lower AFRs showed a maximum efficiency of 0.609 at 60% substitution before dropping significantly at higher ratios, as illustrated in Figure 10(d). This higher peak efficiency at lower AFRs can be attributed to the richer fuel mixture, which, up to a certain substitution level, benefits from the thermal moderation and improved combustion stability provided by biogas [9].

(a) Indicated mean effective pressure against substitution ratio of reformed biogas

(b) Gross indicated power (kW) against substitution ratio of reformed biogas

(c) Combustion efficiency against substitution ratio of reformed biogas

(d) Thermal efficiency against substitution ratio of reformed biogas

Fig. 10. Impact of reformed biogas on the (a) Indicated mean effective pressure (b) Gross indicated power (c) Combustion efficiency (d) Thermal efficiency with varying air-fuel ratios

3.6 Effect of Reformed Biogas Substitution Ratio with Differences of Equivalence Ratio on Emissions

Similar to the previous sub-chapter of 3.5, both the inlet temperature, which is equal to 350K and 5100 J/cycle and the total energy input provided to the engine are considered constants per cycle. Also, it is expected that the 9-bar inlet pressure will remain constant throughout each cycle. Additionally, Table 10 and Figure 11 describe the emissions characteristics under varying air-fuel ratios.

Table 10
Result of the reformed biogas replacement ratio on emissions with varying air-fuel ratio

Inlet temperature - 350K; Inlet pressure - 9 bar; Air-fuel ratio - 1.00			
Reformed biogas substitution (%)	Emission index nitrogen oxide (NOₓ) at exhaust valve opening (g/kW-h)	Carbon oxide at exhaust valve opening (g/kW-h)	Unburnt hydrocarbon at exhaust valve opening (g/kW-h)
20.0%	0.444	92.604	2.117450
40.0%	0.467	80.858	0.380466
60.0%	0.844	57.411	0.000118
80.0%	0.635	85.300	0.980000
Inlet temperature - 350K; Inlet pressure - 9 bar; Air-fuel ratio - 0.80			
Reformed biogas substitution (%)	Emission index nitrogen oxide (NOₓ) at exhaust valve opening (g/kW-h)	Carbon oxide at exhaust valve opening (g/kW-h)	Unburnt hydrocarbon at exhaust valve opening (g/kW-h)
20.0%	36.674	5.025	1.473770
40.0%	34.733	0.827	0.007318
60.0%	34.956	0.503	0.000024
80.0%	0.000	26775.100	2767.850000
Inlet temperature - 350K; Inlet pressure - 9 bar; Air-fuel ratio - 0.60			
Reformed biogas substitution (%)	Emission index nitrogen oxide (NOₓ) at exhaust valve opening (g/kW-h)	Carbon oxide at exhaust valve opening (g/kW-h)	Unburnt hydrocarbon at exhaust valve opening (g/kW-h)
20.0%	45.083	1.644	0.61231
40.0%	38.929	0.627	0.05550
60.0%	21.300	0.004	0.01400
80.0%	0.000	36650.000	3862.27000
Inlet temperature - 350K; Inlet pressure - 9 bar; Air-fuel ratio - 0.40			
Reformed biogas substitution (%)	Emission index nitrogen oxide (NOₓ) at exhaust valve opening (g/kW-h)	Carbon oxide at exhaust valve opening (g/kW-h)	Unburnt hydrocarbon at exhaust valve opening (g/kW-h)
20.0%	5.937	0.524	0.33680
40.0%	3.421	0.015	0.18390
60.0%	0.817	0.033	0.13167
80.0%	0.000	131859.000	14361.70000

NOx emissions increased significantly with higher biogas substitution ratios and lower AFR values, as shown in Figure 11(a). According to Figure 11(a), at AFR 1.0, NOx emissions rose from 0.444 g/kW-h at 20% to 0.635 g/kW-h at 80%, on the other hand, lower AFRs saw a more dramatic increase, with emissions nearly reaching zero at 80% substitution for AFR 0.4. This trend is primarily due to the thermal NOx formation mechanism, which is highly sensitive to combustion temperatures. At higher biogas substitution ratios, the increased number of inert gases like CO2 in biogas initially helps to moderate combustion temperatures, reducing NOx formation [21]. However, at lower AFRs, the fuel mixture becomes richer, leading to higher combustion temperatures that can promote NOx formation despite the presence of CO_2 [9]. At lower AFRs, the richer mixture and the increased thermal effect result in a more dramatic increase in NOx emissions, reaching nearly zero at 80% substitution for AFR 0.4, indicating that at extremely high substitution and low AFRs, the dilution effect might significantly suppress NOx formation due to insufficient oxygen.

CO emissions varied widely, with lower AFR values showing significantly higher CO emissions at higher biogas substitution ratios, as depicted in Figure 11(b). At higher AFRs, CO emissions decreased with increasing biogas substitution, which can be attributed to the improved oxidation of CO due to the thermal moderation provided by the inert gases in biogas. Figure 11(b) depicts that at AFR 1.0, CO emissions reduced from 92.604 g/kW-h at 20% substitution to 85.300 g/kW-h at 80%. However,

at lower AFR values, CO emissions spiked significantly at higher biogas substitution ratios. This spike can be explained by incomplete combustion caused by the excessive dilution of the air-fuel mixture with inert gases, leading to a significant increase in CO emissions [12]. At AFR 0.4, CO emissions soared to 131859 g/kW-h at 80% substitution, reflecting severe combustion inefficiency and poor oxidation conditions.

UHC emissions generally decreased with higher biogas substitution and lower AFR values, as indicated in Figure 11(c). At AFR 1.0, UHC emissions fell from 2.117 g/kW-h at 20% to 0.980 g/kW-h at 80%. At AFR 0.4, UHC emissions peaked significantly at higher substitution ratios. This reduction is due to the improved combustion efficiency resulting from the presence of CO_2 in biogas, which helps to moderate the combustion process and ensure more complete burning of hydrocarbons. Nevertheless, at lower AFR values, UHC emissions peaked significantly at higher substitution ratios. This increase in UHC emissions at lower AFRs can be attributed to the richer fuel mixture combined with excessive dilution from inert gases, leading to incomplete combustion and higher levels of unburnt hydrocarbons [9].
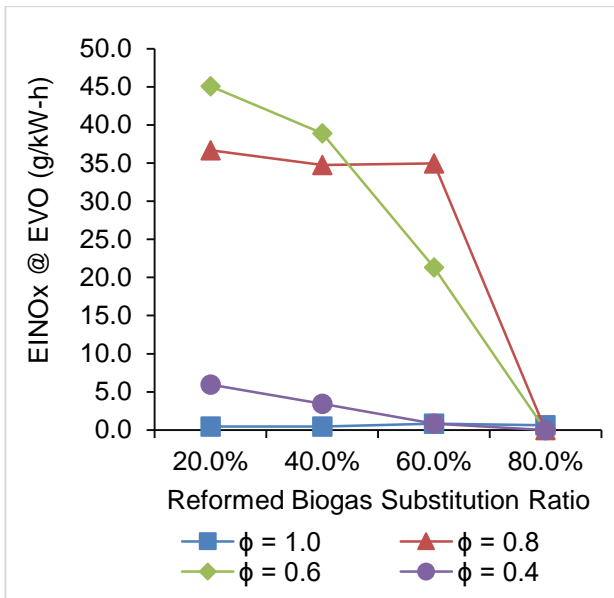
(a) Emission index nitrogen oxide at exhaust valve opening against substitution ratio of reformed biogas
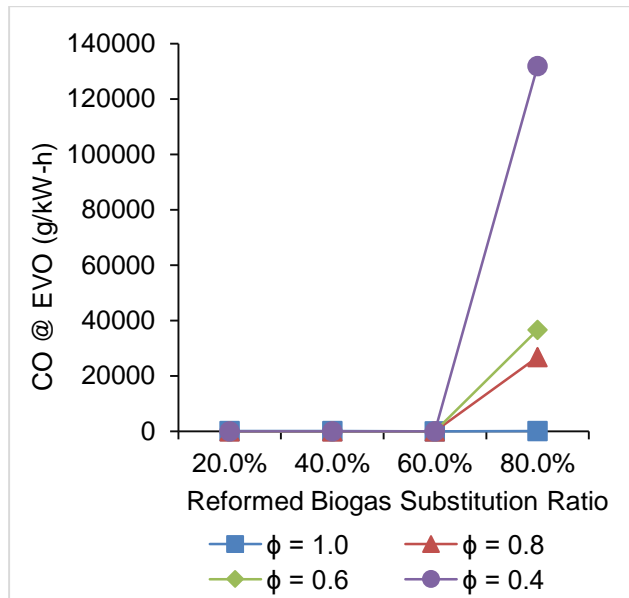
(b) Carbon oxide at exhaust valve opening against substitution ratio of reformed biogas
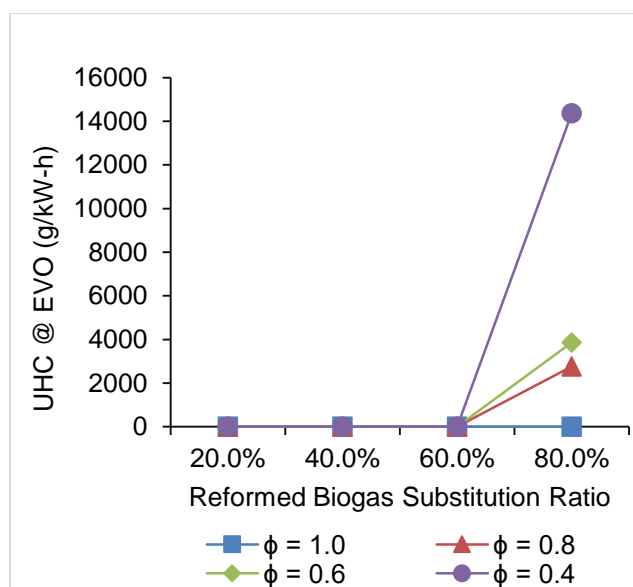
(c) Unburned hydrocarbon at exhaust valve opening
against substitution ratio of reformed biogas

Fig. 11. Impact of reformed biogas on the (a) Emission index NO$_x$ (b) Carbon oxide (c) Unburnt hydrocarbon at exhaust valves opening with varying air-fuel ratios

3.7 Practical Application of Optimised Dual-Fuelled Engine's Parameters

The application of reformed biogas as a renewable fuel in dual-fuel internal combustion engines presents both environmental benefits and economic challenges. Biogas, primarily composed of methane, is recognized for its potential to mitigate greenhouse gas emissions when used as an alternative to fossil fuels [6,11]. However, the transition to biogas requires careful optimization of combustion parameters to enhance performance while minimizing emissions [5]. One of the significant challenges in implementing biogas in dual-fuel engines is the retrofitting of existing diesel engines. This process often necessitates costly modifications, including the installation of advanced fuel injection systems and sensors for monitoring fuel composition [11]. Additionally, biogas purification is crucial to remove impurities such as hydrogen sulphide and carbon dioxide, which adds to operational costs [6]. For small-to-medium-sized enterprises (SMEs), these financial burdens can be daunting without supportive measures like government incentives or carbon credit systems [6]. Moreover, the performance of dual-fuel engines can decline at higher biogas substitution rates. Research indicates that while biogas can lead to reductions in harmful emissions, the engine's efficiency and power output may decrease with increased biogas proportions [5]. This performance degradation could deter industries from fully adopting biogas technology. To mitigate these barriers, effective policies that provide subsidies for renewable energy integration and promote sustainable practices are crucial. Such measures could significantly alleviate the financial burden on companies transitioning to biogas [6]. In conclusion, while reformed biogas offers a promising pathway for sustainable energy, the economic and technical challenges associated with its implementation in dual-fuel internal combustion engines must be strategically addressed. Continued research and development, alongside supportive policy frameworks, are essential for maximizing the environmental benefits of biogas utilization.

4. Conclusions

4.1 Conclusion

This study aims to develop a detailed Computational Fluid Dynamics (CFD) model for simulating the combustion of biogas generated from Palm Oil Mill Effluent (POME) in dual-fuel engines. CFD simulations are used to evaluate how different biogas components affect optimal combustion conditions and to optimize the combustion system by adjusting variables such as inlet temperature, intake pressure and air-fuel ratio. The research results have successfully achieved these goals, providing profound insights into the performance and emission characteristics of dual-fuel engines using reformed biogas.

Firstly, the development of CFD models has made it possible to comprehensively simulate biogas combustion, highlighting the complex dynamics involved. This model indicates that the indicated mean effective pressure (IMEP) and gross indicated power continue to decrease with the increase of biogas substitution rate, which is attributed to the lower calorific value of biogas and the higher content of inert gases such as CO_2. These results emphasize the challenge of maintaining engine performance while increasing biogas substitution rates.

Secondly, the evaluation of different biogas components through CFD simulation revealed key insights into combustion efficiency and thermal efficiency. At lower substitution rates, combustion efficiency remains relatively high, but significantly decreases at higher substitution rates, especially at lower air-fuel ratios. This is due to the increased presence of inert gases hindering complete combustion. The thermal efficiency shows the optimal substitution range, reaching its peak at around 60% biogas substitution rate. Beyond this range, the efficiency will decrease due to excessive fuel dilution and incomplete combustion.

Thirdly, optimizing the combustion system by adjusting intake temperature, intake pressure and air-fuel ratio has a significant impact on engine performance and emissions. With the increase in biogas substitution rate, higher intake temperature intensifies the decrease in IMEP and gross indicated power. The findings also indicated that while NOx emissions increased with higher biogas substitution and lower air-fuel ratios, CO and unburnt hydrocarbons (UHC) emissions generally decreased. This was due to the improved combustion efficiency facilitated by the thermal moderation effect of CO_2 in biogas.

4.2 Future Research

Future research should focus on several key areas to enhance the performance and feasibility of biogas utilization in dual-fuel engines:

i. <u>Exploring Biogas Compositions:</u> Future studies could experiment with varying the composition of biogas, especially investigating the effects of trace elements like hydrogen sulphide (H_2S), carbon monoxide (CO) and water vapour, which may affect combustion dynamics. Such research would help develop more tailored purification processes for biogas and refine combustion strategies for different compositions.

ii. <u>Long-Term Engine Performance:</u> There is a need for long-term performance assessments of engines running on biogas-diesel blends to better understand engine durability, maintenance requirements and overall reliability under prolonged operation. This could also help identify wear-and-tear patterns that occur due to the altered combustion properties of biogas, particularly with high nitrogen or CO_2 content.

iii. <u>Industrial Integration:</u> Further research could investigate the integration of biogas in different industrial applications, including its use in heavy-duty machinery, power generation systems and marine engines. The scalability of biogas technologies for large-scale industrial use is a critical area that remains relatively underexplored.

iv. <u>Hybrid and Alternative Fuel Systems:</u> Investigating biogas-hydrogen blends could provide a path forward for improving engine efficiency while reducing emissions. Research on fuel flexibility and advanced combustion techniques, such as homogeneous charge compression ignition (HCCI), could also optimize the performance of dual-fuel engines using biogas.

Acknowledgement

References

[1] Aziz, Md Maniruzzaman A., Khairul Anuar Kassim, Moetaz ElSergany, Syed Anuar, M. Ehsan Jorat, H. Yaacob, Amimul Ahsan and Monzur A. Imteaz. "Recent advances on palm oil mill effluent (POME) pretreatment and anaerobic reactor for sustainable biogas production." *Renewable and Sustainable Energy Reviews* 119 (2020): 109603. https://doi.org/10.1016/j.rser.2019.109603

[2] Alrbai, Mohammad, Adnan Darwish Ahmad, Sameer Al-Dahidi, Ahmad M. Abubaker, Loiy Al-Ghussain, Ali Alahmer and Nelson K. Akafuah. "Performance and sensitivity analysis of raw biogas combustion under homogenous charge compression ignition conditions." *Energy* 283 (2023): 128486. https://doi.org/10.1016/j.energy.2023.128486

[3] ANSYS Inc. "ANSYS Forte Theory Manual." *ANSYS Inc.*, (2017).

[4] Assad, Mohamad and Oleq Penazkov. "Comprehensive analysis of the operation of an internal combustion engine fueled by hydrogen-containing mixtures." *Energy Reports* 9 (2023): 4478-4492. https://doi.org/10.1016/j.egyr.2023.03.101

[5] Bedoya, Iva´ N. D., Samveg Saxena, Francisco J. Cadavid and Robert W. Dibble. "Numerical analysis of biogas composition effects on combustion parameters and emissions in biogas fueled HCCI engines for power generation." In *Internal Combustion Engine Division Fall Technical Conference*, vol. 44427, pp. 423-440. 2011. https://doi.org/10.1115/ICEF2011-60120

[6] Belinska, Stefaniia, Peter Bielik, Izabela Adamičková, Patrícia Husárová, Svitlana Onyshko and Yanina Belinska. "Assessment of Environmental and Economic-Financial Feasibility of Biogas Plants for Agricultural Waste Treatment." *Sustainability* 16, no. 7 (2024): 2740. https://doi.org/10.3390/su16072740

[7] Bundele, Hiresh, Caneon Kurien, Penmatsa Sandeep Varma and Mayank Mittal. "Experimental and computational study on the enhancement of engine characteristics by hydrogen enrichment in a biogas fuelled spark ignition engine." *International Journal of Hydrogen Energy* 47, no. 71 (2022): 30671-30686. https://doi.org/10.1016/j.ijhydene.2022.07.029

[8] Cameretti, Maria Cristina, Roberta De Robbio, Ezio Mancaruso and Marco Palomba. "CFD study of dual fuel combustion in a research diesel engine fueled by hydrogen." *Energies* 15, no. 15 (2022): 5521. https://doi.org/10.3390/en15155521

[9] Feroskhan, M., Saleel Ismail, Gobinath Natarajan, Sreekanth Manavalla, TM Yunus Khan, Shaik Dawood Abdul Khadar and Mohammed Azam Ali. "A comprehensive study of the effects of various operating parameters on a biogas-diesel dual fuel engine." *Sustainability* 15, no. 2 (2023): 1232. https://doi.org/10.3390/su15021232

[10] Ghenai, Chaouki and Isam Janajreh. "Combustion of renewable biogas fuels." *J. Energy Power Eng* 9, no. 10 (2015): 831-843. https://doi.org/10.17265/1934-8975/2015.10.001

[11] Glivin, Godwin, M. Edwin and S. Joseph Sekhar. "Techno-economic studies on the influences of nonuniform feeding in the biogas plants of educational institutions." *Environmental Progress & Sustainable Energy* 37, no. 6 (2018): 2156-2164. https://doi.org/10.1002/ep.12892

[12] Gupta, Priyank, Caneon Kurien and Mayank Mittal. "Biogas (a promising bioenergy source): A critical review on the potential of biogas as a sustainable energy source for gaseous fuelled spark ignition engines." *International Journal of Hydrogen Energy* 48, no. 21 (2023): 7747-7769. https://doi.org/10.1016/j.ijhydene.2022.11.195

[13] Gupta, Sachin Kumar and Mayank Mittal. "Analysis of cycle-to-cycle combustion variations in a spark-ignition engine operating under various biogas compositions." *Energy & Fuels* 33, no. 12 (2019): 12421-12430. https://doi.org/10.1021/acs.energyfuels.9b02344

[14] Hernandez, Borja and Mariano Martin. "Optimization for biogas to chemicals via tri-reforming. Analysis of Fischer-Tropsch fuels from biogas." *Energy conversion and management* 174 (2018): 998-1013. https://doi.org/10.1016/j.enconman.2018.08.074

[15] Hosseini, Seyed Ehsan and Mazlan Abdul Wahid. "Development of biogas combustion in combined heat and power generation." *Renewable and Sustainable Energy Reviews* 40 (2014): 868-875. https://doi.org/10.1016/j.rser.2014.07.204

[16] Ismail, Najib Aminu, Mazlan Abdul Wahid, Aminuddin Sa'at, Abubakar Shitu and Mohammed Bashir Abdulrahman. "Effect of Recirculation Ratio on the Combustion Characteristics of an Asymmetric Swirling Flameless Combustor using Biogas." *Journal of Advanced Research in Fluid Mechanics and Thermal Sciences* 108, no. 1 (2023): 52-65. https://doi.org/10.37934/arfmts.108.1.5265

[17] Jagadish, C. and Gumtapure Veershetty. "Experimental Studies of Biogas in a Single Cylinder Diesel Engine by Dual Fuel Mode of Operation." *Applied Mechanics and Materials* 895 (2019): 109-114. https://doi.org/10.4028/www.scientific.net/AMM.895.109

[18] Lopes, Shailesh Martin, Robert Furey and Pat Geng. "Calculation of heating value for diesel fuels containing biodiesel." *SAE International Journal of Fuels and Lubricants* 6, no. 2 (2013): 407-418. https://doi.org/10.4271/2013-01-1139

[19] Hussain, Shaik Magbul, Dr B. Sudheer Prem Kumar and K. Vijaya Kumar Reddy. "CFD analysis of combustion and emissions to study the effect of compression ratio and biogas substitution in a diesel engine with experimental verification." *International Journal of Engineering Science and Technology* 4, no. 2 (2012): 473-492.

[20] Mahmod, Safa Senan, Shalini Narayanan Arisht, Jamaliah Md Jahim, Mohd Sobri Takriff, Jian Ping Tan, Abdullah Amru Indera Luthfi and Peer Mohamed Abdul. "Enhancement of biohydrogen production from palm oil mill effluent (POME): A review." *International Journal of Hydrogen Energy* 47, no. 96 (2022): 40637-40655. https://doi.org/10.1016/j.ijhydene.2021.07.225

[21] Mahmoodi, Reza, Mortaza Yari, Jafar Ghafouri and Kamran Poorghasemi. "Effect of reformed biogas as a low reactivity fuel on performance and emissions of a RCCI engine with reformed biogas/diesel dual-fuel combustion." *International Journal of Hydrogen Energy* 46, no. 30 (2021): 16494-16512. https://doi.org/10.1016/j.ijhydene.2020.09.183

[22] Marcoberardino, Gioele Di, Dario Vitali, Francesco Spinelli, Marco Binotti and Giampaolo Manzolini. "Green hydrogen production from raw biogas: A techno-economic investigation of conventional processes using pressure swing adsorption unit." *Processes* 6, no. 3 (2018): 19. https://doi.org/10.3390/pr6030019

[23] Ravi Chandran, Meveeqhen. "Simulation Study on Utilisation of Biogas from Palm Oil Mill Effluent (POME) as Fuel for Diesel Generator Set." IRC, 2020.

[24] Puduppakkam, Karthik V., Long Liang, Chitralkumar V. Naik, Ellen Meeks, Sage L. Kokjohn and Rolf D. Reitz. "Use of detailed kinetics and advanced chemistry-solution techniques in CFD to investigate dual-fuel engine concepts." *SAE International Journal of Engines* 4, no. 1 (2011): 1127-1149. https://doi.org/10.4271/2011-01-0895

[25] Rajani, Ahmad, Kusnadi, A. Santosa, A. Saepudin, S. Gobikrishnan and D. Andriani. "Review on biogas from palm oil mill effluent (POME): challenges and opportunities in Indonesia." In *IOP Conference Series: Earth and Environmental Science*, vol. 293, no. 1, p. 012004. IOP Publishing, 2019. https://doi.org/10.1088/1755-1315/293/1/012004

[26] Riboldi, Luca and Olav Bolland. "Overview on pressure swing adsorption (PSA) as CO2 capture technology: state-of-the-art, limits and potentials." *Energy Procedia* 114 (2017): 2390-2400. https://doi.org/10.1016/j.egypro.2017.03.1385

[27] Sowmya, H N, Sunil Kumar, Saurav Kumar and Ujjwal Kumar. "Generation Of Biogas Using Food Waste." *International Research Journal of Modernization in Engineering Technology and Science*, (2021). www.irjmets.com

[28] Kumar, K. Sunil, P. Yogesh, Hari Narayana Vemulakonda and Koyyana Hemanth Kumar. "Performance, combustion and emissions characteristics of palm biodiesel blends in CI engines." *Materials Today: Proceedings* (2023).

[29] Wijeyakulasuriya, Sameera, Ravichandra S. Jupudi, Shawn Givler, Roy J. Primus, Adam E. Klingbeil, Mandhapati Raju and Ashwin Raman. "Multidimensional modeling and validation of dual-fuel combustion in a large bore medium speed diesel engine." In *Internal Combustion Engine Division Fall Technical Conference*, vol. 57274, p. V001T01A006. American Society of Mechanical Engineers, 2015. https://doi.org/10.1115/ICEF2015-1077

[30] Wongfaed, Nantharat, Prawit Kongjan, Poonsuk Prasertsan and O. Sompong. "Effect of oil and derivative in palm oil mill effluent on the process imbalance of biogas production." *Journal of Cleaner Production* 247 (2020): 119110. https://doi.org/10.1016/j.jclepro.2019.119110

[31] Zirkler, Doreen andre Peters and Martin Kaupenjohann. "Elemental composition of biogas residues: Variability and alteration during anaerobic digestion." *Biomass and bioenergy* 67 (2014): 89-98. https://doi.org/10.1016/j.biombioe.2014.04.021